Techno-Economic Feasibility Study of a Novel Process for Simultaneous Concentration of TDS and Recovery of Clean Water from Acid Mine Drainage

OSM Cooperative Agreement Number S16AC20062

FINAL REPORT

Reporting Period Start Date: 10/01/2016

Reporting Period End Date: 09/30/2018

Vadim Guliants (PI) and Joo-Youp Lee (co-PI)

December 2018

Department of Chemical and Environmental Engineering

University of Cincinnati

Cincinnati, OH 45221-0012

Disclaimer

ABSTRACT

This applied science project explored the techno-economic feasibility of a new membrane distillation (MD) process to selectively remove >90% of water from acid mine drainage (AMD) and concentrate total dissolved solid (TDS) employing five promising commercial membranes (two Polypropylene (PP), two Polytetrafluoroethylene (PTFE) and one Polyvinylidene fluoride (PVDF)). Among all commercial membranes tested, 0.45 μm pore PP membrane exhibited the highest water flux (ca. 62 kg/h*m^2) and achieved 90% water recovery under optimal batch MD conditions.

Long-term open-loop continuous MD testing of the 0.45 μm pore PP membrane was conducted utilizing simulated AMD feed (TDS = 900 mg/l, pH = 2.4) which was concentrated 10-fold under optimal steady-state MD conditions and resulted in a high and stable water flux of ~45 kg/h*m^2. The results of these tests indicated that the PP membrane would need to be replaced once every 150 days under real process conditions.

Our economic study of a scaled up open-loop continuous MD process to treat 1 million gallons of AMD per day indicated that such frequency of membrane replacement is expected to have a very minor impact on the overall process economics. The cost analysis of the MD plant was performed for two major components of capital cost and annual operating cost, and for four different energy sources, including local utility, photovoltaic, solar thermal, wind, and natural gas. The economic analysis indicated pipelined natural gas and local electricity to be the most economical energy sources for heating AMD water that result in total treatment costs of \$0.476/m^3 and \$0.607/m^3 of AMD, respectively. However, by 2030 these AMD treatment costs are expected to be comparable to the costs based on renewable energy (\$0.702/m^3) due to increasing natural gas prices and decreasing renewable energy costs, especially for photovoltaic (PV). These costs compare favorably with our estimates of combined costs of chemical treatment and floc handling and disposal of precipitated metal hydroxides, which were estimated to be in the range of \$0.250-\$0.500 m^3 of AMD.

LIST OF GRAPHICAL MATERIALS

INTRODUCTION

Acid mine drainage (AMD) occurs when sulfide minerals in rocks, predominantly iron sulfides pyrite and marcasite (FeS_2), are exposed to oxidizing conditions in coal and metal mining, highway construction, and other large-scale excavations (Jacobs and Testa, 2014). Upon exposure to water and oxygen, sulfide minerals are oxidized to form acidic iron- and sulfate-rich drainage. Approximately 20,000 km of streams and rivers in the United States are degraded by AMD. About 90% of the AMD reaching streams originates in abandoned surface and deep mines, which results in continual contamination of surface water and groundwater resources. Besides the presence of iron and sulfate ions and low pH, AMD also contains trace metals that are classified as priority pollutants and regulated by USEPA to parts-per-billion or parts-per-trillion levels due to their toxicity (Neuman et al. 2014; USEPA, 2012a) (Table 1). As the data shown in Table 1 indicate, the levels of some of these metals in groundwaters within the United States may significantly exceed their chronic and even acute levels for criteria maximum freshwater concentrations.

Table 1. Pollutant concentrations (μg/l) in groundwaters (GW) and AMD (Neuman et al. 2014), and maximum contaminant levels (MCLs) for regulated toxic species and their goals (MCLGs) (USEPA 2012a).

Species	GW (μg/l)	MCL (μg/l)	MCLG (μg/l)
arsenic	0.01-2,100	10	0
beryllium	<0.01	4	4
cadmium	0-180	5	5
chromium	0.06-2,740	100	100
copper	1.3-2.8	13	9
iron	<6,000,000*	300-3,000**	-
lead	0-5.6	15	0
mercury	0-0.01	2	2
selenium	0.6-20	50	5
silver	9.0-330	3.2	-
zinc	0.1-240	120	120
sulfate	120,000-35,000,000*	<250**	-

* specifically in AMD ** taste threshold (USEPA 2011).

Typical AMD chemical treatment system consists of an inflow pipe or ditch, a storage tank or bin holding the acid-neutralizing chemical, a means of controlling its application rate, a settling pond to capture precipitated metal oxyhydroxides, and discharge point (Skousen 2014). The latter is the location where National Pollutant Discharge Elimination System (NPDES) compliance established by the Clean Water Act (CWA) of 1972 is monitored. Chemicals used to treat AMD include hydrated lime, pebble quicklime, caustic soda, soda ash briquettes, and ammonia. Under low-flow conditions, pebble quicklime and ammonia are the most cost-effective, while under high-flow conditions hydrated lime and pebble quicklime are the most economical treatment chemicals due to their lower reagent costs and high neutralization efficiency as compared to other options. Therefore, each AMD is evaluated and treated with the optimal chemical from the standpoints of environmental soundness, efficiency and cost.

Coagulants and flocculants may be used in water treatment where retention time in sedimentation ponds is insufficient for metal precipitation, but they add significant consumable and capital costs to the AMD treatment process. Besides, the floc, the metal hydroxides collected in settlement ponds after chemical treatment, are disposed of in abandoned deep mines, which also adds very significant costs. For example, Lovett and Ziemkiewicz (1991) estimated ammonia chemical costs for a site in West Virginia at $72,000 per year and floc handling costs at $486,000

per year corresponding to a cost of $6.25/yd^3 for floc handling and disposal on that site. Several mine operators further observed that floc handling and disposal may cost up to $15/yd^3. Due to its high water content and the sheer volume of material, floc handling costs frequently exceed chemical costs several-fold.

However, metals dissolved in AMD are difficult to remove by current methods of chemical precipitation due to fundamental limitations. As mentioned above, these current methods employ hydrated lime or other common bases to neutralize the low pH and form insoluble metal hydroxides. While the pH neutralization in AMD requires significant amounts of consumable bases, *the conversion of dissolved metals into insoluble hydroxides is incomplete* as shown in by Higgins *et al*. (2009) (Figure 1). Moreover, because AMD contains multiple combinations of acidity and dissolved metals, each AMD is unique and its treatment by these chemicals varies widely from site to site. For example, the AMD from one site may be completely neutralized and contain no dissolved metals at a pH of 8.0, whereas another site may still have dissolved metal concentrations that do not meet effluent limits even after the pH has been raised to 10 (Skousen 2014). This represents a significant environmental challenge, because the concentrations of many toxic metals in treated AMD by far exceed permissible discharge levels (Table 1 and USEPA, 2009 & 2011).

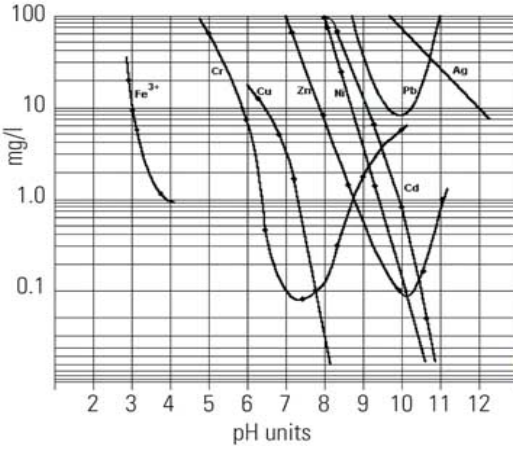

Figure 1. Solubility of metal hydroxides (Higgins *et al*., 2009).

Treatment of AMD by Membrane Distillation

Clean water that is safe for surface discharge can be separated from AMD efficiently and economically by *membrane distillation* (MD). MD is a thermally driven separation process (Figure 2), where water from a liquid AMD feed stream at a higher temperature (e.g., 50-80 ℃) is transported as vapor across micropores of a hydrophobic membrane where it is condensed into a liquid distillate stream at a lower temperature (e.g., 5-30 ℃). All nonvolatile components present in AMD (i.e., sulfuric acid and all dissolved metal cations and anions) can be concentrated by MD for subsequent chemical treatment.

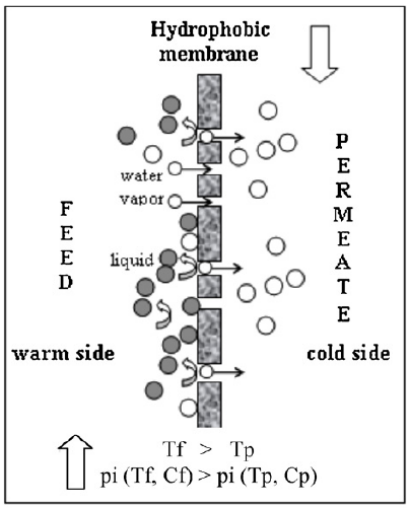

Figure 2. The warm AMD feed is flown across a hydrophobic microporous membrane resulting in water vapor diffusion to and condensation on the cold permeate side. MD concentrates all non-volatiles present in AMD, e.g., sulfuric acid, metals and anions.

The MD membranes have low resistance to mass transfer and low thermal conductivity to prevent heat loss across the membrane. In addition, they have good thermal stability, and high resistance to chemicals, such as acids and bases. Liquid entry pressure (LEP) is a significant membrane characteristic. The feed liquid must not penetrate the membrane pores; so the pressure applied should not exceed the limit, or LEP, where the liquid (i.e. aqueous solution) penetrates the hydrophobic membrane. Commercial hydrophobic microporous (0.1–0.6 μm) membranes made

from polytetrafluoroethylene (PTFE), polypropylene (PP) or polyvinylidene fluoride (PVDF) possess high LEP values of 200-500 kPa that effectively prevents intrusion of the liquid feed and distillate into membrane pores (Alkhudhiri et al. 2012). Finally, the membrane thickness between 30–60 μm and porosity (defined as the volume of the pores divided by the total volume of the membrane) of 30 to 85% were found to be optimal to achieve high water flux.

MD is a non-isothermal process, where two main heat transfer mechanisms are known to occur: latent heat and conduction heat transfer. The thermal efficiency in MD can be specified as the ratio of latent heat of vaporization to the total (latent and conduction) heat. Previous studies (Al-Obaidani et al. 2008) indicated that the thermal efficiency can be improved by increasing the feed temperature, feed flow rate and membrane thickness. Around 50–80% of the total heat flux across the membrane is considered to be latent heat, whereas the remainder of heat is lost by conduction through the membrane (Fane et al. 1987). It was observed (Alklaibi and Lior 2005) that by increasing the feed temperature from 40 to 80 °C, the thermal efficiency increased by 12%, whereas the salt concentration has a marginal effect on the thermal efficiency.

With regard to energy consumption, a simple energy balance based on mass flows of hot and cold streams (Criscuoli et al. 2008) can be used to compute the energy consumption for MD using different flow configurations. Since the vaporization phenomenon occurs at the membrane hot surface and condensation at the opposite side of the membrane, thermal boundary layers are established on both sides of the membrane. The temperature difference between the liquid-vapor interface and the bulk is called temperature polarization. The effect of thermal boundary layer to total heat transfer resistance of the system is measured by temperature polarization. Working at a high feed and distillate flow rates minimizes the hydrodynamic and thermal boundary layer resistances and maximizes the heat-transfer coefficient resulting in a higher permeate flux (Srisurichan et al. 2006). The fluid cross-flow velocity increases with the volumetric flow rate, which in turn enhances the convective heat-transfer coefficient and results in contraction of the thermal boundary layer and a significant reduction of the temperature polarization effect (Chen et al. 2009). Lastly, it is observed that the extent of membrane fouling in MD is significantly lower than that encountered in conventional pressure-driven membrane separation, such as RO.

The energy requirements for MD are moderate: it requires low-grade heat to warm the feed solution to 70-80 °C, and energy to operate a chiller to keep the distillate stream at 15-25 °C; and energy to continuously pump feed and distillate solutions tangentially to the MD membrane. In the absence of on-site utilities, as may be the case for many AMD sources, these energy requirements for MD may be provided by solar power as demonstrated in recent studies (e.g., Duong et al. 2015; Zhao et al. 2013). Moreover, the chilling power requirements may be significantly reduced by using available AMD streams and ponds as natural heat sinks for the distillate stream. If significant corrosion of metal heat exchangers exposed to AMD is expected, the distillate water can also be ponded and used as a natural heat sink for the distillate stream.

Therefore, the major advantages of the MD process for treating AMD are the following:

- It can remove >90% of water thereby considerably decreasing the volume of AMD for subsequent processing.
- It can handle concentrated AMD up to solubility limits of dissolved metals.
- It can concentrate sulfuric acid and dissolved metals >10-fold, which will improve the efficiency and cost-effectiveness of downstream chemical treatment options.
- It requires relatively low energy inputs, which can be provided on site by solar power.

Objectives

The main objective of this applied science project was to explore the techno-economic feasibility of a new MD process to selectively remove >90% of water from AMD and concentrate TDS. It focused on (i) identifying the best membranes and MD process conditions that result in the highest water flux and lowest flux of TDS; (ii) preliminary capital and operating cost estimates for such novel MD process conducted on a representative scale; and (iii) comparison of these costs with cost estimates of current chemical precipitation methods.

EXECUTIVE SUMMARY

This *applied science project* explored the techno-economic feasibility of a novel membrane distillation (MD) process to concentrate metals present in acid mine drainage (AMD), such as iron, etc., and produce clean water for safe discharge to the environment. We investigated (i) concentration of total dissolved solids (TDS) and recovery of clean water from simulated AMD by MD employing commercial hydrophobic microporous membranes (two PTFE from GE Osmonics and Pall Corporation; two PP from 3M/Cuno; and one PVDF from Millipore Corporation) as a function of AMD acidity, TDS content, as well as process temperature and flowrate in a batch process; (ii) open-loop continuous operation of the MD process; (iii) membrane fouling and MD operation for up to 30 days on stream under best experimental conditions identified in tasks (i) and (ii).

Among all commercial membranes tested, 0.45 μm pore PP membrane exhibited the highest water flux (ca. 62 kg/h*m^2) and achieved 90% water recovery under optimal batch MD conditions (heater: 90 °C; chiller: 10 °C; feed/distillate flowrate: 30 l/h) when using simulated AMD containing Fe^{2+}, SO_4^{2-}, Na^+, etc., at TDS ~ 46 g/l and pH = 2.0. The final distillate at 90% water recovery was characterized by neutral pH and low TDS content (TDS = 35 mg/l and pH = 6.49). This membrane experienced fouling after repeated batch MD tests which was manifested in increased TDS content in the distillate. The fouling was investigated by scanning electron microscopy (SEM), which revealed high atomic Fe/S and low Na/S<2 ratios inside the membrane cross-section. It was proposed that the molecular oxygen diffusing from the cold distillate stream across the air gap was responsible for the Fe^{2+} oxidation and the deposition of sulfate-depleted Fe^{3+}/Fe^{2+} (oxy)hydroxide at the liquid-vapor interface inside the membrane, which lead to a drop in water flux as well as membrane wetting and feed penetration to the distillate stream.

Further open-loop continuous MD testing was conducted for AMD compositions representative of the Appalachian region, which are characterized by lower TDS concentrations. Specifically, historical AMD compositions from the FR0126 site on Raccoon Creek were used as basis for simulated AMD feed (TDS ~ 9.8 g/l and Fe^{2+}) employed in these initial tests. However, these tests were conducted by maintaining the feed concentration at ~98 g/l corresponding to 90% water recovery by adding deionized water to the feed at the same rate as it was removed by the MD process. The 0.45 μm pore PP membrane experienced rapid water flux decline after 4 hours under such process conditions, which was due to membrane fouling by the oxidized Fe^{3+}/Fe^{2+} (oxy)hydroxide. Fe^{2+} was used to prepare these simulated AMD sources since Fe was reported to be predominantly in the ferrous state in natural sources at low pH.

Subsequent MD testing was conducted for real AMD feed collected from Raccoon Creek location at Carbondale doser in Nelsonville, OH, which had TDS ~900 mg/l and pH = 3.20. Besides much lower TDS concentration than that in the historical data, our UV-vis

spectrophotometric analysis (3500-Fe-B Phenatroline method) indicated that 70% of all Fe in this Raccoon Creek water was Fe^{3+} suggesting that this creek water would result in insignificant Fe^{3+}/Fe^{2+} (oxy)hydroxide fouling. However, extensive batch MD testing revealed that the 0.45 μm pore PP membrane experienced rapid flux decline when the water recovery reached ~75%, which SEM and X-ray diffraction demonstrated to be due to the deposition of needle-like gypsum crystals. Based on the composition of the creek water, dissolved gypsum was expected to becomes saturated at circa (ca.) 50% water recovery, which was in agreement with experimental observations of the flux decline and gypsum scaling above 75% water recovery. Fe^{2+} oxidation in this creek water as it aged was also found to play a role in raising dissolved Ca^{2+} and SO_4^{2-} concentrations and increasing gypsum and calcite scaling of the PP membrane during batch MD tests. The gypsum and calcite scaling observed after quick batch MD tests was easily removed and water flux recovered by a brief wash with dilute acid (0.01 M H_2SO_4 or HNO_3). However, acid washing was ineffective in restoring the water flux after open-loop continuous MD testing using aged creek water that was concentrated 10-fold, because it had untypically high dissolved Ca^{2+} and SO_4^{2-} concentrations as compared to the historical data for all Raccoon Creek sites, including FR0126.

In order to conduct long-term open-loop continuous MD testing of the PP membrane under realistic and reproducible conditions that minimize feed ageing, we utilized a simulated Raccoon Creek composition (TDS = 900 mg/l, pH = 2.4, and containing Fe^{3+}) which was concentrated 10-fold under optimal steady-state MD conditions and resulted in the water flux of ~45 kg/h*m^2. The water flux began to decline after 4-5 days of open-loop continuous MD testing, which was recovered by membrane washing with 0.01 M HNO_3. After 15 days of operation, the TDS in the distillate increased, while the water flux could not be recovered by the acid wash. These observations suggested that the membrane surface partially lost its hydrophobic character due to acid treatment and/or scaling. However, it should be noted that in this long-term test, the contact volume of concentrated feed normalized to membrane area and time was 371 l/h m^2, while in a full-scale process, this parameter is expected to be ca. 10 times lower (36.4 l/h m^2). This indicated that the PP membrane may be need to be replaced once every 150 days under real process conditions.

Our economic study of an open-loop continuous MD process to treat 1 million gallons of AMD per day indicated that such frequency of membrane replacement is expected to have a very minor impact on the overall process economics. The cost analysis of the MD plant was performed for two major components of capital cost and annual operating cost, and for four different energy sources, including local utility, photovoltaic, solar thermal, wind, and natural gas. The economic analysis indicated pipelined natural gas and local electricity to be the most economical energy sources for heating AMD water that result in total treatment costs of \$ 0.476/m^3 and \$0.607/m^3 of AMD, respectively. However, by 2030 these AMD treatment costs are expected to be comparable to the costs based on renewable energy (\$ 0.702/m^3) due to increasing natural gas prices and decreasing renewable energy costs, especially for PV. These costs compare favorably with our estimates of combined costs of chemical treatment and floc handling and disposal of precipitated metal hydroxides, which were estimated to be in the \$0.324-\$0.880 m^3 of AMD.

EXPERIMENTAL

Process flow diagram

The bench-scale set-up shown in Figures 3 and 4 was used in batch tests in this applied science project to establish MD as a viable technology to treat AMD. This set-up was further modified for the proposed open-loop continuous mode operation described below and shown in Figure 5.

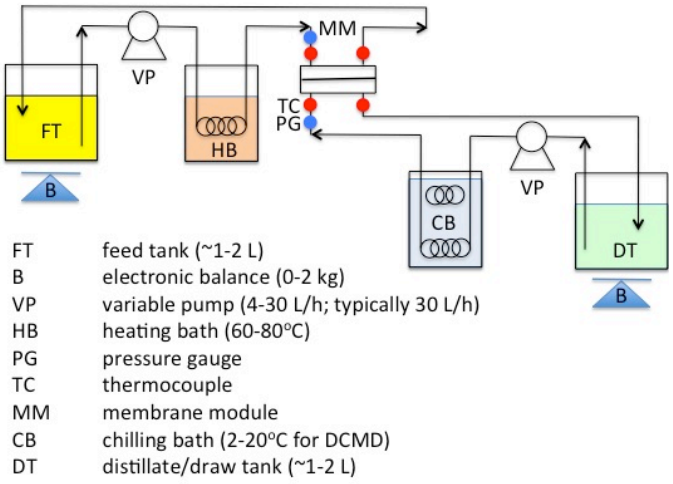

Figure 3. Schematic diagram of batch MD setup.

MD tests conducted in batch mode

Besides the PTFE membrane reported in preliminary MD studies, we investigated 5 additional membranes that also showed very high water flux of >35 kg/h*m^2 and high liquid entry pressures of 25-40 psig in our preliminary studies:

- PTFE QP909 membrane (0.45 µm pores) from GE Osmonics
- PTFE PTF045LD0A membrane (0.45 µm pores) from Pall Corporation
- Two PP membranes (0.2 and 0.45 µm pores) from 3M/Cu no Company
- PVDF IPVH10100 membrane (0.45 µm pores) from EMD Millipore Corporation.

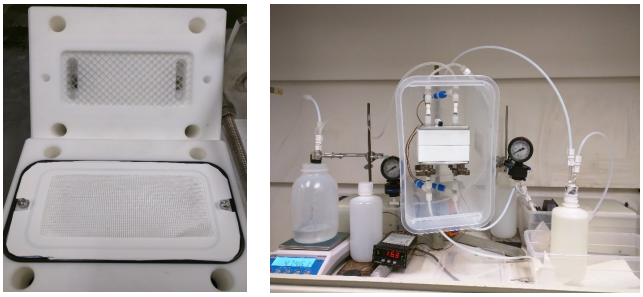

Figure 4. (Left) open CF042P cell showing a feed spacer (top) and permeate carrier (bottom); the outer edges of a flat membrane located underneath permeate carrier are also visible. (Right) MD setup showing a loaded cell with connections to peristaltic pumps and solution containers.

These MD studies were conducted in a batch mode under optimal experimental conditions described above employing a proposed simulated AMD stream containing representative concentrations of toxic metals at pH 2 (Table 3). This solution was made up from soluble metal sulfates (Cd, Cr, Fe, and Zn), sodium arsenate, sodium selenate, and adjusted to pH 2 with dilute sulfuric acid. We monitored inlet/outlet pressures and temperatures for both the AMD feed and distillate (i.e., purified water) and determined the water flux from the mass changes in the feed and distillate. Specifically, we investigated the impact of feed/distillate temperature (feed: 70-85 °C; distillate: 12-25 °C) and flow rate (20-35 l/h) on the water flux in these studies. Each batch test was conducted until 90% of water was recovered, at which point the pH and metal concentrations in

Table 3. Simulated pH 2 AMD stream.

Species	µg/l
arsenic	50
cadmium	50
chromium	200
iron	5,000,000
selenium	100
zinc	200
sulfate	30,000,000

the distillate (purified water) were determined by pH, TDS and Inductively Coupled Plasma Mass Spectrometer (ICP-MS) measurements (for the toxics). The main objective of these tests was to confirm that the final concentrations of these toxic metals in the distillate did not exceed the maximum contaminant levels (MCLs) (USEPA 2012a) shown in Table 1.

MD tests conducted in open-loop continuous mode

The best MD membranes identified in the tests described above were investigated in an open-loop continuous process (Figure 5). In an open-loop continuous process, fresh simulated AMD was introduced into a tank and concentrated AMD withdrawn at a rate to maintain a constant volume of the AMD feed in the tank, while purified water (i.e., the distillate) will be also taken out at a rate to maintain it at a constant volume in the distillate tank. However, the majority of these longer-term tests was conducted in a closed-loop continuous mode, where purified water recovered by MD was recycled at the same flowrate to the feed side to maintain the AMD concentration at a level corresponding to 90% water recovery. The water flux in the MD process was measured under such conditions by the respective volumetric rates of the AMD addition and purified water withdrawal (or purified water recycle rate). The dissolved metal concentrations in the distillate were checked by ICP-MS to confirm that they do not exceed MCLs (Table 1). The major objective of these tests was to investigate short-term performance (up to 90 days of operation) of the MD membranes in the proposed process, which also enabled to examine the occurrence of membrane fouling, its rate, nature and impact on water fluxes. Our ultimate goal was to demonstrate the capability of the closed-loop continuous operation to recover at least 90% of purified water at pH~5.65, while maintaining the concentrations of toxic metals in this water below their maximum contaminant levels (MCLs) (USEPA 2012a) shown in Table 1.

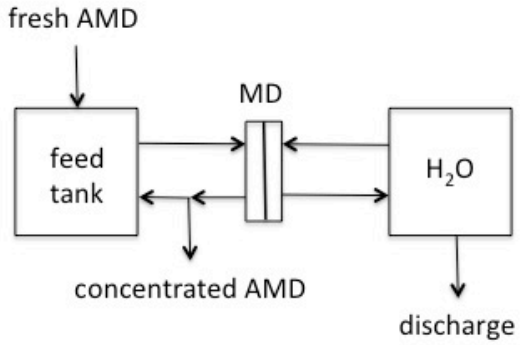

Figure 5. MD testing in open-loop continuous mode.

Facilities, Equipment and Infrastructure to be used for Proposed Work

The following state-of-the-art equipment contained in the co-PIs' laboratories and the College of Engineering Materials Characterization Center at UC was employed for the studies of the MD process to recover purified water from AMD:

- Hydrothermal Synthesis Autoclaves, Ovens, Heaters, Circulation Baths, Stirrers, Shakers.
- Furnaces for Heat Treatments up to 1,700 °C in Controlled Atmosphere.
- Agilent 7700 Inductively Coupled Plasma Mass Spectrometer
- Dispersive Raman System (ISA T64000) with Several Lasers, Microscope and *in situ* Cell
- Temperature-Programmed Desorption, Oxidation, and Reduction Apparatuses
- Cross-Flow CF042P Membrane Cell and Components for either MD or FO Tests
- Shimadzu Gas Chromatograph/Mass Spectrometer System
- Dynamic Light-Scattering Photometer (Malvern Instruments)
- Micromeritics TriStar 3000 Porosimeter
- Micromeritics ASAP 2020 Adsorption Porosimeter

- Computer Automated TA Instruments DSC/DTA/TGA Unit for Studies of Phase Transformations from -196 to 1,500 °C.
- Philips X'Pert MPD θ–θ Powder Diffractometer System.
- FEI-Philips XL-30 FEG ESEM with Capabilities for *in situ* Studies to 1,500 °C.
- Philips CM20 200 kV TEM with EDAX NX-2 Ultra-Thin Window EDS System (Capable of Element Detection to Boron), a High-Resolution TV System and Associated Hardware/Software/Peripherals.
- Fully Equipped Machine Shop with Technicians and Instrumentation Specialist for Help in Apparatus Construction.

Energy and mass balances

The mass balances during MD operations were determined directly by continuously weighing process solutions. The mass balances for individual cations present in these streams were determined with the help of ICP-MS elemental analysis, which is highly accurate down to sub-ppb level concentrations. The energy balances for the MD process were determined on the basis of inlet/outlet temperature and volumetric rate measurements for all process streams as a function of test time as reported previously by Criscuoli et al. (2008).

A process flow diagram (PFD) showing the mass and energy balances was developed based on the experimental data obtained from the closed-loop continuous process configuration. For this purpose, a steady-state process simulator package, PRO/II, was used to construct the mass and energy balances along with essential physical and thermodynamic properties and then to scale up the proposed process for typical range of AMD flows reported in the literature, e.g., 1,000 gal/min (Neuman et al. 2014). Although the phase equilibrium can be predicted using the package, the separation of water, metals and minerals relies heavily on the performance of MD membranes. Therefore, the total and component mass balances was closed based on the experimental performance data. An energy balance was also shown for the entire process including MD process, pumps, heat exchangers, chiller, etc., which was used to evaluate process economics. The energy balance was used to calculate the MD energy requirements (i.e., heating, cooling and electricity).

After the mass and energy balances were constructed for the experimental set-up, the balances were taken for a representative AMD stream. The PFD showing the mass and energy balances for a scaled-up process clearly showed the detailed process conditions including water flow rates, compositions of metals and minerals, temperatures, pressures, enthalpy, and essential physical properties (e.g., density, viscosity, heat capacity, ionic strength, pH, etc.). Then the energy requirements for the entire process were estimated in comparison with those reported for a typical AMD chemical treatment system (Skousen 2014).

Establishing baseline data

Data and results were recorded in a manner consistent to achieve patent protection:

- Water flux and other separation results from the prescribed protocols, including electronic data
- Membrane characterization results from the prescribed protocols
- Detailed simulated AMD composition and preparation methods
- Detailed experimental procedures employed in MD tests
- Schedule updates and plans for the subsequent period

Quality Assurance/Quality Control

The U.S. Environmental Protection Agency (USEPA) reference method for the determination of trace elements in waters and wastes by inductively coupled plasma – mass spectrometry (USEPA method 200.8, revision 5.4, 1994) and the technical assistance document (TAD) for this method were used extensively for the method description. The USEPA quality assurance requirements for state and local water monitoring and assessment program (USEPA 2003) were used in the development of effective quality assurance procedures. We used various statistical process controls to fulfill the requirements of the quality. The experiments were triple checked for the accuracy of the data. We collected several calibration data for the MD process to fulfill the quality requirements of the final product and used several safety procedures according to the EPA regulations in our lab.

This project utilized heavy metal salts and their dilute aqueous solutions that are known to pose certain health risks. The levels of these heavy metals in used solutions were determined by the USEPA reference method for the determination of trace elements in waters and wastes by inductively coupled plasma – mass spectrometry (USEPA method 200.8, revision 5.4, 1994). The technical assistance document (TAD) for this method was used extensively for the method description. The USEPA quality assurance requirements for state and local water monitoring and assessment program (USEPA 2003) were used in the development of effective quality assurance procedures. We used various statistical process controls to fulfill the quality requirements. Moreover, we followed all the safety requirements specified by the University of Cincinnati (UC) chemical safety committee for dealing with heavy metal salts and their dilute solutions in this study. All project personnel were trained to be familiar with the hazards of the chemicals used in this research gas, their proper handling and emergency procedures. This included documented general laboratory safety training, laboratory-specific safety training and personal protective equipment training (contained in the UC Laboratory Chemical Safety Manual). Fume hoods, gas cabinets and exhausted enclosures had an airflow measuring device and visual and audible alarms that signify low airflow conditions. A process hazard analysis was performed regularly to ensure the protection of people, property and the environment (either on or off site) from dangerous conditions involving the metal salts and their solutions.

Techno-economic analysis

During the project period, performance tests were carried out for the water flux and metal separation using various MD membranes. Based on these data, process economic analysis was carried out by updating mass and energy balances for a scaled-up process. A techno-economic analysis was carried out by taking into account the membrane separation performances, desired recovery of water, desired separation of metals and minerals, membrane areas and lifetime, energy requirements for heating, cooling and electricity. The information on these factors was obtained from the performance data and mass and energy balances. Based on the operating conditions, materials required for individual unit operations were determined for estimating a capital cost for the process. In addition, based on further technical data on the membrane performances, the membrane areas for MD was estimated for a footprint requirement.

The techno-economic analysis task consisted of the following three steps: 1) creating a detailed process-based techno-economic model for the proposed system including the proposed innovative elements based on lab experimental datasets; 2) coupling a variability and sensitivity analysis to determine the key influential factors (such as desired separation requirements of water

flux and metal concentrations, footprint requirement, and others) for energy, water, environmental and economic performances; and 3) comparing the performances of the proposed conceptual design with conventional processes. Overall, the goal of the analysis was to provide an understanding of technical, environmental and economic performances of the proposed membrane-based separation system.

RESULTS AND DISCUSSION

A1. Assembly of MD system, water flux testing of representative membranes, and morphological and chemical composition characterization of used MD membranes

Table 4 shows a comparison of the MD water flux results obtained in our preliminary study and the initial study employing a new MD system. We selected two membranes that showed a high water flux in our preliminary study for this comparison conducted at similar MD conditions. The water flux (Jw) was calculated as a function of time from the mass changes during MD as follows:

$$Jw = \Delta m/M_A\Delta t$$

where Δm is the mass change during a time interval Δt, and M_A is the membrane area.

Table 4. Comparison of MD water flux results observed in our preliminary study with those for a new MD system (conditions: DI water used for both the feed and distillate; flow rate: 20 l/h for both feed and distillate; chiller temperature: 4 °C; heater temperature: 90 °C).

	Membrane	Manufacturer	Water flux (kg/h*m^2)
Preliminary MD study	PTFE QP909	GE Osmonics	41
	PTFE PTF045LD0A	Pall Corporation	40
	PP membrane (0.2 micron)	3M/Cuno Company	42
	PP membrane (0.45 micron)	3M/Cuno Company	48
	PVDF IPVH10100	Millipore Corporation	41
New MD system	PP membrane (0.2 micron)	3M/Cuno Company	57
	PTFE QP909	GE Osmonics	48

As can be seen from the results of our preliminary MD study, most membranes showed the water flux of ca. 40 kg/h*m^2 when DI water was used as a feed, while in the new MD system noticeably higher fluxes were observed, i.e., 57 kg/h*m^2 for polypropylene (PP) possessing 0.2 micron pores, and 48 kg/h*m^2 for the PTFE QP909 membrane. The observed increases of the water flux may be explained by greater temperature differences between the feed and distillate side as described below. According to Alklaibi and Lior (2005), it was observed that by increasing the feed temperature from 40 to 80 °C, the thermal efficiency increased by 12%, whereas the salt concentration had a marginal effect on the thermal efficiency. In our preliminary study, the average temperature differences between the feed and distillate side were 57 °C for PP and 60 °C for PTFE membranes, while for the tests conducted in the new MD setup, higher temperature differences of 67.7 °C and 68.1 °C were achieved for the PP and PTFE membranes, respectively. We were able to achieve the greater temperature differences and higher water fluxes because we used more efficient SS heater exchangers instead of glass heat exchangers used in preliminary studies.

Figure 6 shows the water flux as a function of time using DI water and simulated wastewater as a feed for the two best membranes. The simulated wastewater contained Ca^{2+}, Mg^{2+}, Na^{+}, NO_3^{-}, Cl^{-} and SO_4^{2-} ions (Table 5).

Table 5. Concentrations of matrix ions in simulated wastewater.

Ion	Concentration (µg/l)
Ca^{2+}	87,267
Mg^{2+}	1,800,000
Na^{+}	2,373,833
NO_3^{-}	353,000
Cl^{-}	8,334,721
SO_4^{2-}	781,000

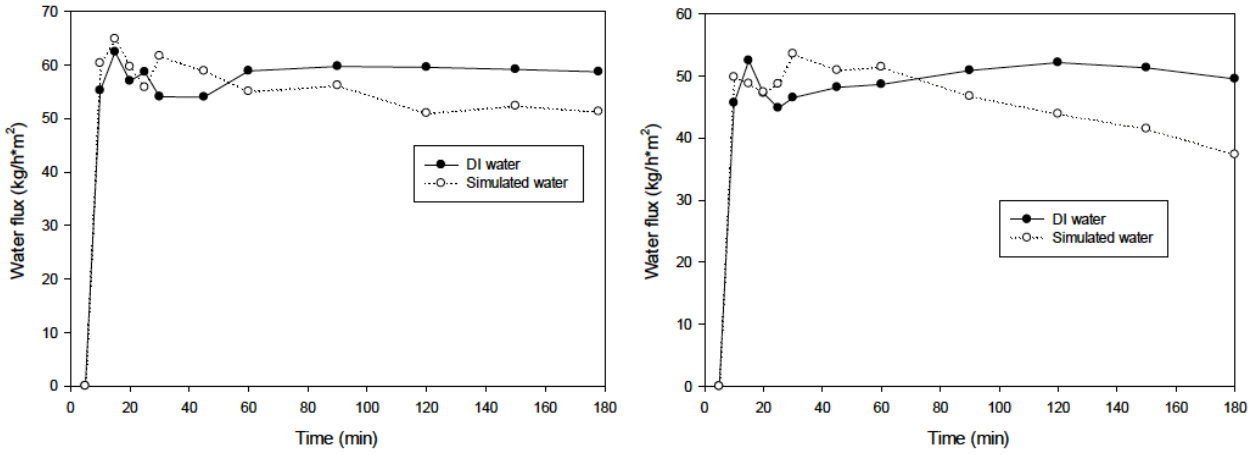

Figure 6. The water flux as a function of time in MD test using (left) a PP membrane (3M/Cuno, 0.2 micron pore size) and (right) PTFE membrane (QP909, GE Osmonics).

When DI water used as a feed, the water flux remained essentially unchanged as a function of time. When the simulated wastewater was used as a feed, the water flux began to decrease slightly after ca. 1 h of operation. In the case of the PP membrane, the flux gradually decreased from 58 to 53 kg/h*m^2, while this decrease was greater for the PTFE membrane (QP909), from 52 to 40 kg/h*m^2 after 3 h of operation. This decrease in water flux was expected because the saturation water pressure decreased with increasing concentration of salts in the feed solution as a function of time. The observed flux differences for the PP and PTFE membranes may be explained by several factors, such as differences in the pore size, membrane thickness, as well as morphological and structural differences between the PTFE and PP membranes. Further studies are planned to identify the optimal membranes and process conditions to accomplish the objectives of this project.

Significant Events

1. The MD bench-scale set-up was assembled as shown in Figure 3.
2. Compare performance of the new MD system to that used in preliminary MD experiments.
3. For this comparison, 2 membranes that showed promising water flux in our preliminary studies were chosen and tested in MD of deionized water in a batch mode for several weeks.
4. The MD test was conducted using simulated wastewater in a batch mode for several weeks.

Accomplishments

1) Assemble a bench-scale MD system (100% accomplished).

2) Perform water flux testing of representative membranes in batch MD for several weeks (100% accomplished)

3) Conduct morphological and chemical composition characterization of used MD membranes by Scanning Electron Microscopy/Energy-dispersive X-ray spectroscopy (SEM and EDS) for the presence of fouling and scaling (No fouling and scaling was observed during MD tests; SEM/EDS not conducted: 0% accomplished)

4) Quality control and reproducibility of water flux (100% accomplished).

A2. Determine water flux and toxics concentrations in batch MD using simulated AMD; characterize fouling in used membranes; identify best MD membranes and process conditions.

The same five microporous hydrophobic membranes described in *Thrust A1* were employed to determine the water flux using simulated AMD prepared using soluble metal salts (Table 6). The simulated AMD prepared had a natural pH of 3.6 and contained a small amount of some undissolved material. The pH was further adjusted to 2 by adding sulfuric acid. At pH 2, the solution became transparent and was used as the MD feed. The amount of sulfuric acid added to adjust the pH corresponded to 955 mg/l, while the AMD solution already contained 30,000 mg/l of sulfate anions. Four different representative process conditions were employed selected as a function of feed and distillate temperature, flow rates and simulated AMD pH (Table 7).

Table 6. Simulated AMD feed.

IONS	SOURCES	CONC. (µg/l)
Cr	$Cr(NO_3)_3 \times 9H_2O$	200
Zn	$ZnSO_4 \times 7H_2O$	200
As	$Na_2HAsO_4 \times 7H_2O$	100
Se	$Na_2SeO_4 \times 10H_2O$	100
Cd	$CdSO_4 \times 8/3H_2O$	50
Fe	$FeSO_4 \times 7H_2O$	5,000,000
Na	Na_2SO_4, $Na_2HAsO_4 \times 7H_2O$, $Na_2SeO_4 \times 10H_2O$	10,246,000
Nitrate	$Cr(NO_3)_3 \times 9H_2O$	715
Sulfate	Na_2SO_4, $FeSO_4 \times 7H_2O$, H_2SO_4, $ZnSO_4 \times 7H_2O$, $CdSO_4 \times 8/3H_2O$	30,995,000

Table 7. MD process conditions employed.

Condition	Feed T (°C)	Distillate T (°C)	Feed flowrate (l/h)	Distillate flowrate (l/h)	Feed pH
1	90	10	30	30	2
2	90	10	30	20	2
3	80	20	20	20	2
4	90	10	30	30	1

Table 8. Average water flux measured in MD experiments employing simulated AMD.

MEMBRANES	Manufacturer	Condition 1 ($kg/h*m^2$)	Condition 2 ($kg/h*m^2$)	Condition 3 ($kg/h*m^2$)	Condition 4 ($kg/h*m^2$)
PP (0.2 microns)	3M/Cuno Co.	56	53	33	57
PP (0.45 microns)	3M/Cuno Co.	**62**	**50**	**36**	**58**
PTFE QP909	GE Osmonics	46	30	27	45
PTFE PTF045LD0A	Pall Corp.	44	43	29	42
PVDF IPVH10100	Millipore Corp.	35	-	-	

Table 8 shows that the best operating condition was Condition 1 (the feed temperature of 90 °C) and the best membrane was PP (0.45 micron pores) characterized by a high average water flux of 62 $kg/h*m^2$. The flux and water recovery obtained under condition 4 (pH 1) were very similar to those obtained for Condition 1 indicating that lowering the pH does not have a significant effect on these characteristics.

Since the water flux measured for the PVDF membrane from Millipore Corporation was relatively low even under the best process conditions, it was not further tested under Conditions 2 and 3. A significant decrease in the water flux was observed when process conditions were changed from Condition 1 to Condition 3 due to the lower feed temperature (Table 9).

Table 9. Reduction in the water flux observed when changing from Condition 1 to Condition 3.

Membranes	Reduction in Flux (%)
PP (0.2 microns)	41
PP (0.45 microns)	42
PTFE QP909	41
PTFE PTF045LD0A	34

The decrease in the water flux with solute concentration during MD can be explained by the Raoult's law. When non-volatile solutes are added to water, the vapor pressure of the solution is reduced as compared to that of pure water due to a decrease in the water activity. As the feed

loses water to the distillate, the solution becomes depleted in solvent thereby leading to a progressive lowering of vapor pressure:

$$P(\text{solvent}) = x(\text{solvent}) * P^0(\text{solvent})$$

where x is the mole fraction of the solvent and P^o is the pure solvent vapor pressure. This explains the trends in water flux and salt concentration shown in Figures 7-9. The flux decreases as the salt concentration increases over time during MD experiments.

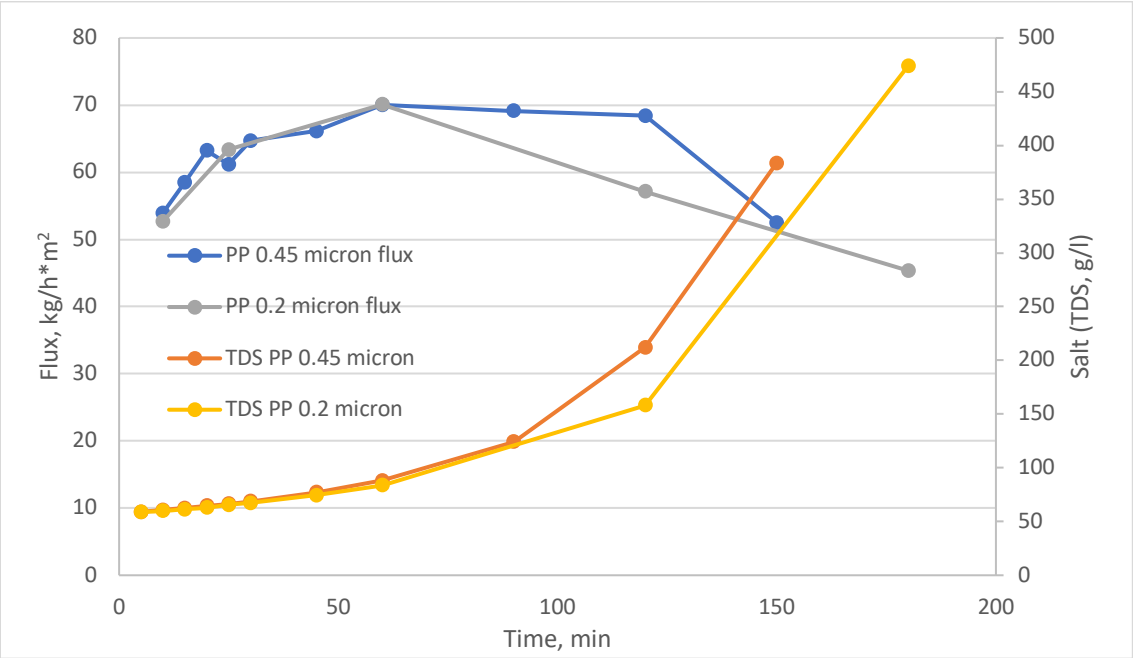

Figure 7. Water flux under Condition 1 and the TDS (g/l) in the feed as a function of time for PP (0.2 microns) and PP (0.45 microns) membranes from 3M/Cuno Company.

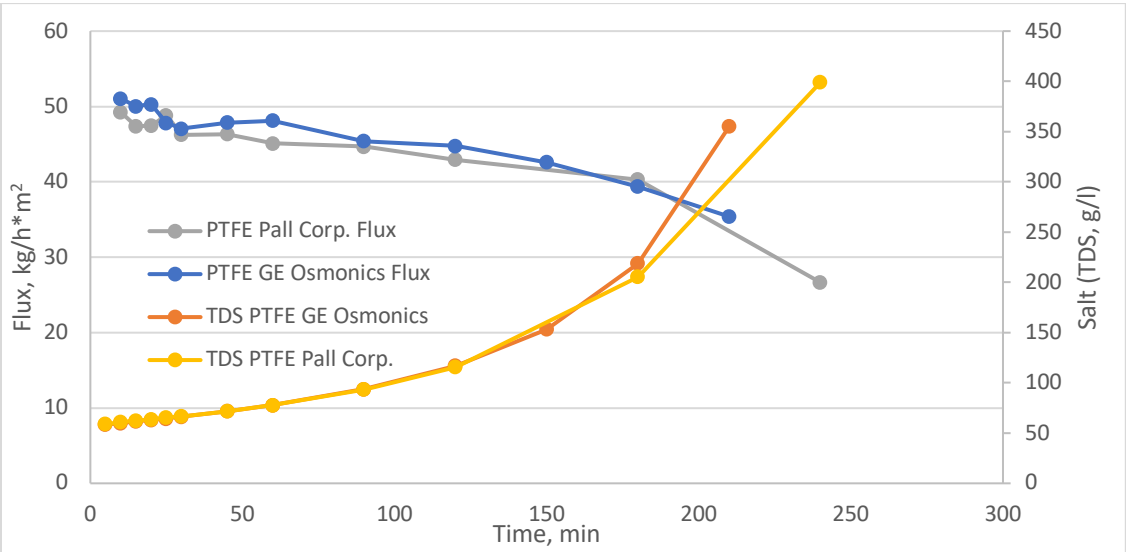

Figure 8. Water flux under Condition 1 and the TDS (g/l) in the feed as a function of time for PTFE QP909 membrane from GE Osmonics and PTFE PTF045LD0A membrane from Pall Corporation.

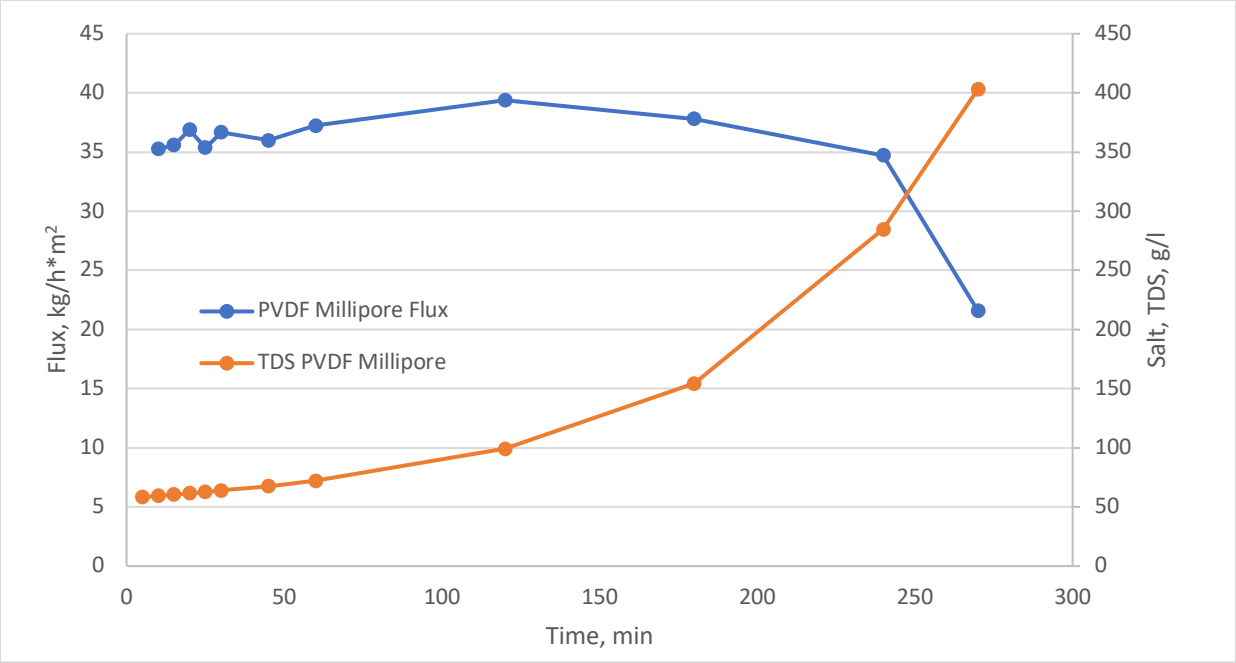

Figure 9. Water flux under Condition 1 and the TDS (g/l) in the feed as a function of time for PVDF IPVH10100 membrane from Millipore Corporation.

Table 10. A summary of the membrane performance.

Membranes	Condition	Initial Feed pH	Initial Feed TDS (mg/l)	Average Flux (kg/h*m^2)	% Water Recovery	Final Distillate pH	Final Distillate TDS (mg/l)
PP (0.45 µm) 3M/Cuno	1	2	46,242	62	87	6.49	35
PP (0.2 µm) 3M/Cuno	1	2	46,242	56	89	3.30	100
PTFE GE Osmonics	1	2	46,242	48	85	6.56	24
PTFE Pall Corporation	1	2	46,242	44	87	2.50	1500
PVDF IVPH10100	1	2	46,242	35	87	6.18	40

The time required to achieve ca. 90% water recovery is an indication of the performance of the membrane. PP membranes (0.2 and 0.45 microns) achieved ~90% water recovery within 3 hours while PTFE and PVDF took longer to achieve this recovery, as seen in Figures 7-9. It should be noted that all membranes maintained significant water flux throughout the entire duration of each MD test, even when the total TDS concentration exceeded 400 g/l. The TDS content in the final distillate was measured using a water quality test meter (Play X Store digital tool with TDS, conductivity (EC), and temperature; 0-9990 part per million (ppm) measurement range; ±2% readout). The ppm units reported by this test meter are essentially the same as mg/l for these very dilute solutions.

Table 10 shows that PP (0.45 microns) from 3M/Cuno Company displayed a high flux, 87% water recovery and very low TDS content in the final distillate. Two membranes (PP 0.2 micron, and PTFE Pall) showed higher TDS and significantly lower pH in the final distillate. We will examine these 2 membranes further in order to understand these differences in behavior.

Significant Events

1) Polypropylene (PP, 0.2 and 0.45 micron pores), 2 polytetrafluoroethylene (PTFE 0.45 micron pores), and polyvinylidene fluoride (PVDF) membranes were employed.
2) The PP membrane containing 0.45 micron pores was the best one displaying a high average water flux of 62 kg/h*m^2 using the simulated AMD under the best process conditions.
3) The best process conditions corresponded to average process ΔT of 61 ^{o} C, and feed and distillate flowrates of 30 l/h.
4) The PVDF membrane displayed the lowest water flux among the membranes tested under the best process conditions employed.
5) All membranes did not exhibit fouling behavior when using simulated AMD as feed.

Accomplishments

1) Conducted the batch MD experiments using five hydrophobic membranes [100% accomplished].
2) Determined the water flux for each membrane under different process conditions [100 % accomplished].
3) Observed the lack of membrane scaling and fouling on the basis of water flux measurements and visual examination [100% accomplished].
4) Identified best membranes and process conditions resulting in high water flux and 90% water recovery from simulated AMD feed [100% accomplished].

A3. Characterize membrane fouling; Identify the best membranes and MD process conditions; Review economic information about relevant MD processes

The three best membranes, PP 0.45 micron from 3M/Cuno Company, PTFE 0.45 micron from GE Osmonics (QP909) and PTFE PTF045LD0A 0.45 micron from Pall Corporation reported in *Thrust A2* were investigated with respect to fouling and scaling under two different MD process conditions employing the same simulated AMD feed solution containing high initial TDS concentration of ~45,000 mg/l. The initial TDS concentration in this simulated AMD was significantly higher than typical TDS content of real AMD streams (see below), which enabled accelerated fouling and scaling tests.

Table 11. MD process conditions employed to study accelerated fouling.

Condition	Heater T, ℃	Cooler T, ℃	Flow rate (feed and distillate), l/h
1	90	10	30
2	80	20	20

Table 11 shows the MD operating conditions employed to study the accelerated membrane fouling. Greater than 90% water recovery was achieved and the water flux reproducibility was also confirmed by repeated MD runs. The water flux for the PP membrane was reproducible within ±1.4 kg/h*m^2. The error bars were higher for the PTFE

membranes because they experienced faster fouling.

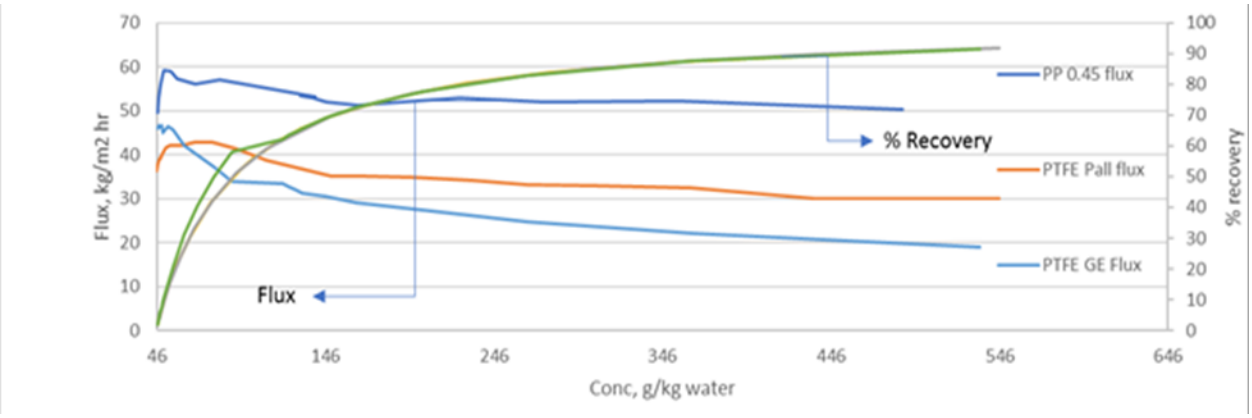

Figure 10. Plots of water flux and % water recovery vs. feed TDS concentration.

In Figure 10, the water recovery curves for the three membranes overlap at high concentrations. Also, from Figure 10, it can be seen that the TDS in the feed at >90% recovery was extremely high. It is remarkable that these membranes displayed considerable water flux under such extreme conditions, e.g., ~ 50 kg/h*m^2 for the PP membrane.

The TDS in the final distillate was measured at the end of every run. Any detectable TDS measured in the distillate above 20 mg/l was used as an indication of membrane fouling. At that point, the membrane was removed from the housing to examine the morphology and chemical composition of foulants presents. The maximum contaminant level (MCL) for TDS in drinking water is 500 mg/l (US EPA 2017). According to World Health Organization (WHO, 2017), water with TDS content less than 600 mg/l is palatable.

Table 12. Results of MD tests performed during accelerated fouling study.

Membrane	Condition	Hours of operation	TDS, mg/l, in the final distillate
PP 0.45	Condition 1 (x2)	6	0
	Condition 2 (x2)	12	34
PTFE GE	Condition 1 (x1)	6	10
	Condition 2 (x1)	10	76
PTFE Pall Corp.	Condition 1 (x1)	6	7
	Condition 2 (x1)	12	65

Table 12 shows the TDS in the distillate and corresponding number of hours each membrane was tested under accelerated fouling conditions. The highest TDS content in the final distillate was observed for the PTFE GE membrane, while the lowest TDS content was observed for the PP 0.45 membrane. The TDS content was also proportional to the total duration of MD tests during which the membranes were exposed to progressively higher TDS content in the feed.

Although these membranes are hydrophobic, the membrane morphology and process conditions can have a significant impact on their surface characteristics. These hydrophobic membranes are characterized by the water contact angles and liquid entry pressures (LEP). The contact angles for PP 0.45 micron (Franken et al. 1987) and PTFE membranes are greater

than 100° (Eykens et al. 2017) corresponding to hydrophobic surfaces. The operating pressure differences of the MD system were kept well below the LEP values in our MD tests. However, the feed stream towards the end of each MD run became highly concentrated, which was further enhanced at the liquid-vapor interface resulting in concentration polarization that likely led to fouling (Shirazi et al. 2010). Each membrane is characterized by a liquid-vapor interface, where the water evaporates through the pore channels. Fouling can cause pore blocking, add a resistance to mass transfer, and reduce surface hydrophobicity leading to wetting and feed penetration through the fouled membrane pathways (Laqbaqbi et al. 2017).

It should be stressed that accelerated fouling observed in these MD tests was due to untypically high Fe and TDS concentrations in the feed solution. Specifically, 5,000 mg/l of iron initially present in this simulated AMD feed was generated by adding ferrous sulfate. This iron can be easily oxidized at the liquid-vapor interface of the membrane by molecular oxygen diffusing from the cold distillate stream. According to our findings below, this oxidized iron oxide/hydroxide can accumulate inside the pores of the membrane (Warsingera et al. 2014). This type of oxidized iron fouling is difficult to remove by simple acid washing because deposited foulants may not be accessible to the acid wash solution. However, the extent of fouling is not expected to be significant for realistic AMD compositions, e.g., those shown in Table 13 for the Appalachian region, where the TDS content is 30-120 times lower.

Table 13. Representative concentrations of major ions in real AMD streams of the Appalachian region and the concentration in simulated AMD feed used in this study.

	Location	**Iron, Fe(II) (mg/l)**	**Sulfate, SO_4^{2-} (mg/l)**	**TDS (mg/l)**	**Reference**
Real AMD Compositions in Appalachian Region	Brubacker run, PA	114	381	560	Larson et al. 2014
	Scalp level, PA	92.3	429	567	
	Sulfur run, PA	102	212	368	
	Summerlee, WV	275	547	877	
	Upper run, PA	383	903	1,500	
Simulated AMD	-	5,000	30,000	45,000	This study

The data shown in Table 13 indicate that the concentration of major ions, iron and sulfate, in the simulated AMD feed is much greater than the concentrations measured in real AMD streams in 5 locations across the Appalachian region. However, the advantage of high TDS content in the simulated feed was that it enabled us to conduct accelerated fouling study.

The morphology and chemical composition of fouled membranes were examined using environmental scanning electron microscopy, ESEM, combined with energy dispersive spectroscopy, EDS (FEI XL30 ESEM and EDS system) at 30 kV and 100x-10,000x magnifications. For the ESEM characterization, the discolored membrane coupons were sputtered with gold prior to imaging to render the surfaces electrically conductive and eliminate surface charging which contributes to imaging artifacts.

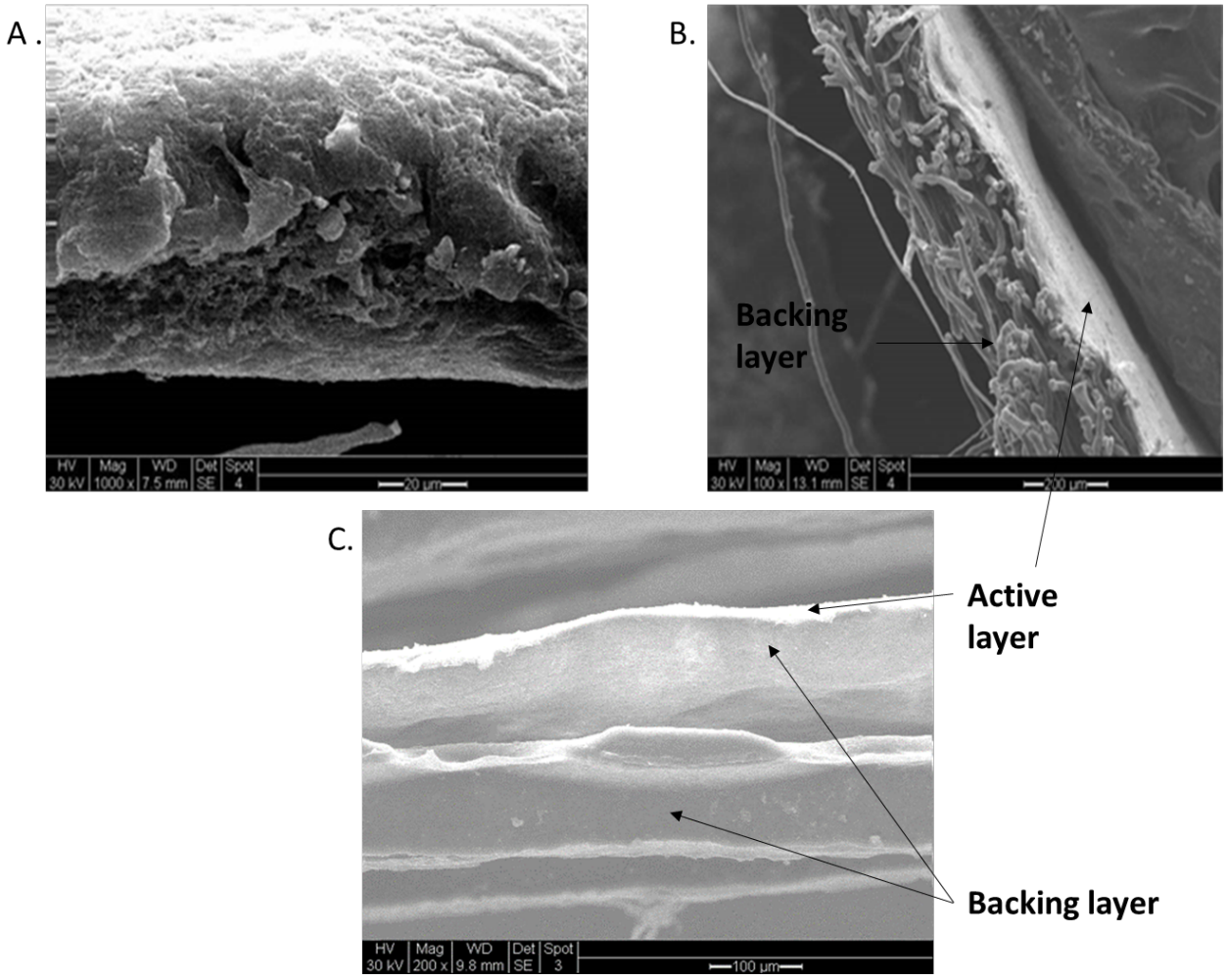

Figure 11. Cross sectional images of A) PP membrane (top left) at 1000x magnification; B) PTFE GE Osmonics membrane (top right) at 100x magnification; C) PTFE Pall Corp (bottom) at 200x magnification.

Figure 11 shows cross sections of the three clean membranes. For the PP membrane (Figure 11A), the feed surface is at the top and the distillate surface is at the bottom of the image. The membrane morphology is the same across the thickness of the PP membrane. The PTFE GE Osmonics membrane has two different morphological regions (Figure 11B). There is a thin PTFE layer facing the MD feed solution and a thick layer of non-woven worm-like PP fibers, that forms the backing of the PTFE layer. In Figure 11C, the PTFE membrane from Pall Corp also has an active layer and two backing layers. The active layer facing the MD feed stream is at the top of the image and the support layers are at the bottom. The support layers in the PTFE Pall membrane contain polyester fibers. The thickness of PTFE GE membrane is wider than the thickness of PP and PTFE Pall membranes, which explains lower water flux observed for this membrane as compared to the other 2 membranes.

The same membrane coupons were analyzed by EDS with respect to the chemical composition of inorganic foulants present. In addition to spot EDS analysis on membrane surfaces, line scans across the cross section of the membranes were collected to determine any variation in composition from the feed to distillate surface which would indicate feed penetration contributing to the distillate TDS.

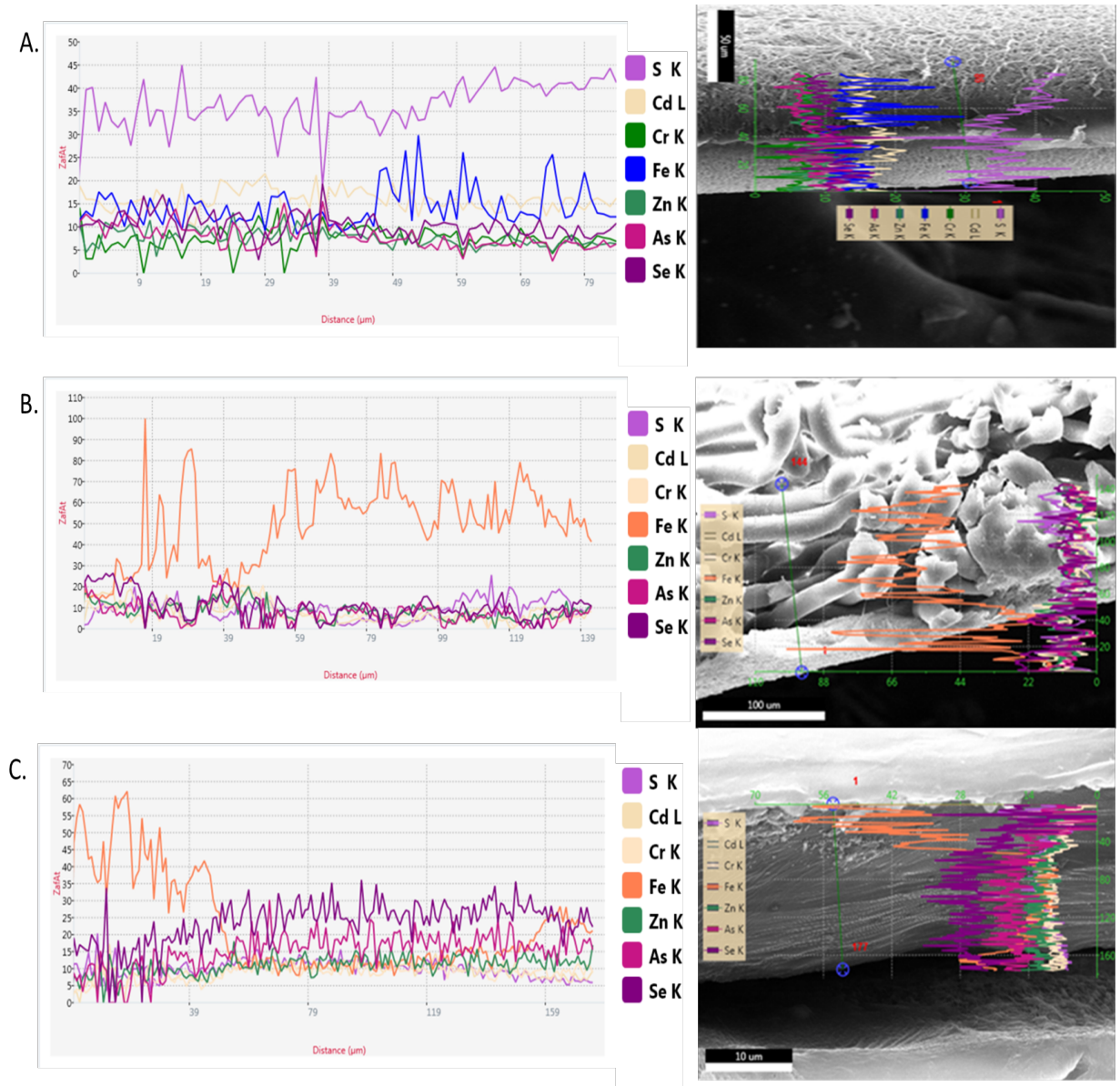

Figure 12. Line scans for the cross-sections of A) PP 0.45; B) PTFE GE; C) PTFE Pall membranes.

The line scans seen in Figure 12 indicate the atomic concentrations (%) of relevant elements with distance in the cross-section. For the line scan shown in Figure 12A, the surface at 0 µm is the distillate surface and the surface at 86 µm is the feed surface of the PP membrane. In Figures 12B and 12C, the surface at 0 µm is the feed surface. Since Fe is expected to be the major foulant, we examined the Fe/S ratios as a further indicator of the chemical nature of Fe foulants. This ratio for the PP membrane was much lower on the feed surface than at the vapor-liquid interface inside the membrane where Fe(II) gets oxidized by molecular oxygen diffusing across air gaps inside the membrane from the cold distillate stream (Table 14). This precipitated oxidized iron present at the vapor-liquid interface can foul the membrane by blocking the pores or causing small defects in the membrane which may allow a small amount of feed to penetrate the membrane resulting in elevated TDS in the distillate.

Table 14. Fe/S ratios in the PP 0.45 membrane from the line-scan atomic concentrations shown in **Figure 13A**.

Location	Feed surface, 86 µm	Liquid-vapor interface, ~49 µm	Distillate surface, 0 µm
Fe/S ratio	0.32	0.90	0.54

The elemental line scans across the PTFE membranes were not used to determine the Fe/S ratios because of their low signal to noise (S/N) ratios (~1). Instead, cross-sectional EDS analysis at different spots was conducted to determine these ratios (Tables 15 and 16).

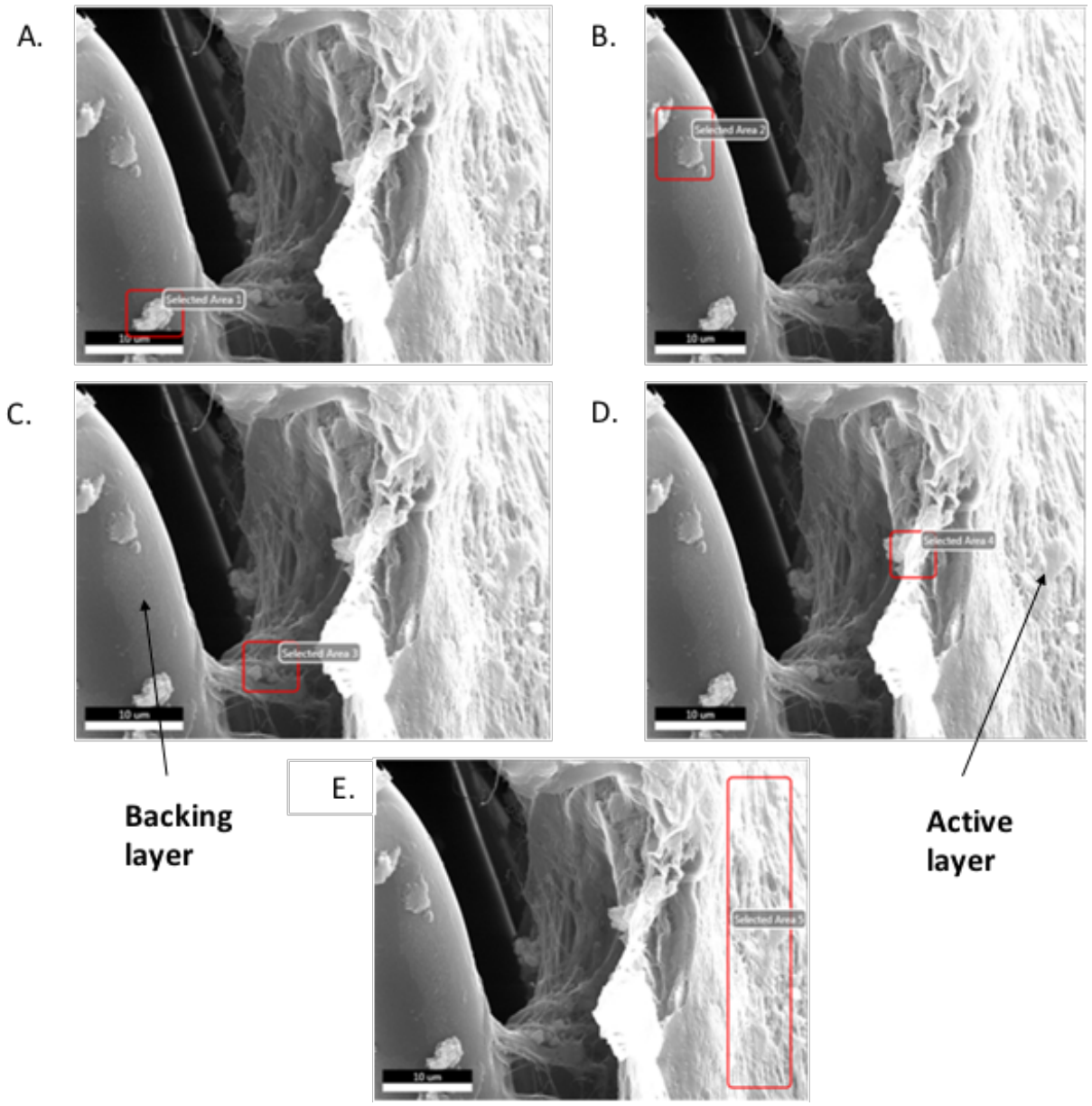

Figure 13. Different cross-sectional areas at the interface between PTFE layer (right side of each image) and fibrous support (left side of each image) in the PTFE GE membrane. (A) and (B) show areas selected in the fibrous backing of the membrane, (C) shows an area selected at the interface; (D) shows an area selected in the active layer closer to the interface; and (E) shows a larger area selected in the active PTFE layer.

Table 15. Fe/S ratios in the PTFE GE membrane in selected areas shown in **Figure 13**.

Location	Fig. 13A	Fig. 13B	Fig. 13C	Fig. 13D	Fig. 13E
Fe/S ratio	2.04	1.02	9.39	2.30	0.108

The extremely high Fe/S ratio found in the interfacial region (Figure 13C) suggested the presence of iron oxide/hydroxide particles containing very little sulfate, while sulfate content in the backing layer of the PTFE GE membrane was significantly higher (Figure 13 and Table 15). Moreover, this ratio was very low in the middle of the active layer indicating the presence of Fe with very low S content. These results qualitatively agreed with the line scan results for the PP membrane, with one notable exception that the liquid-vapor interface for the PTFE GE membrane appears to be located close to the active layer/backing layer interface. We also hypothesize that large, thick PP fibers of the backing in the PTFE GE membrane may partially penetrate the active layer and serve as a conduit for fouling and feed penetration into the distillate stream.

A similar spot analysis was carried out for the fouled PTFE Pall membrane. The Fe/S ratios were analyzed at different locations across the membrane cross-section to understand the fouling behavior (Figure 14 and Table 16).

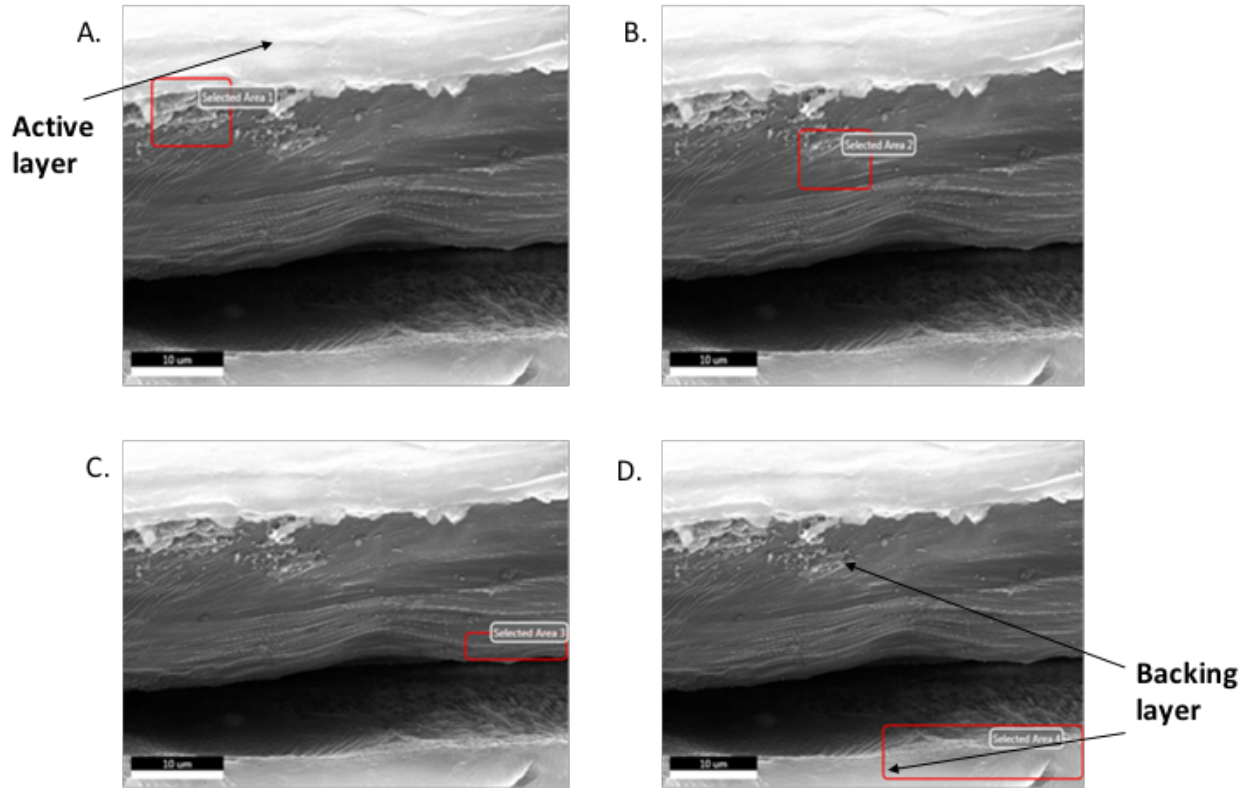

Figure 14. Different cross-sectional areas of PTFE Pall membrane: (A) an area selected close to the interface between the active and backing layers, (B) an area selected in the top backing layer, (C) an area selected close to the interface between the two backing layers, and (D) an area in the bottom backing layer.

Table 16. Fe/S ratios in the PTFE Pall membrane cross-section in selected areas shown in **Figure 14**.

Location	Fig. 14A	Fig. 14B	Fig. 14C	Fig. 14D
Fe/S ratio	2.65	1.07	39.7	1.35

From Tables 14-16, it is evident that the Fe/S ratio reaches the maximum at the liquid-vapor interface, which is located close to the interface between the active and backing layers for the PTFE membranes. These high Fe/S ratios suggest that the primary membrane foulant is oxidized iron oxide/hydroxide. Very high Fe content and TDS of the simulated AMD feed employed in this study caused accelerated membrane fouling, which is expected to be much less significant at realistic concentrations, such as those shown in Table 13. It should be noted that all fouled membranes were also probed by X-ray diffraction and Raman spectroscopy. However, these methods did not yield any insights into the nature of the foulants present due to their low content.

The MD process is an energy-intensive process. The energy required in membrane distillation includes the electrical energy to run the variable pumps and the thermal energy required to heat the feed solution and to cool the distillate. Different MD processes are reported in the literature, for example, MD with heat recovery, MD without heat recovery, solar-powered MD, etc. Water production cost (WPC) depends on the operating costs and the capital costs. Sixty percent (60%) of WPC in MD depends on the source of thermal energy. The WPC with membrane distillation can range from \$0.1/m^3 to \$130/m^3. Although the economic formulas to determine the WPC are similar for many MD systems, these costs depend on multiple factors, which makes them unique for different MD setups. Factors, such as membrane module costs, membrane costs, fouling and membrane life make the WPC different for every MD process. From the literature review, the WPC for MD without heat recovery was found to be \$1.30/m^3 on an average.

Significant Events

1) Accelerated membrane scaling and fouling was studied for 3 membranes: polypropylene, PP 0.45-micron by 3M/Cuno Company; polytetrafluoroethylene, PTFE 0.45-micron by GE Osmonics (QP909); and a new PTFE 0.45-micron membrane (PTF045DL0A) from Pall Corporation by examining their morphology and elemental composition of foulants present after MD tests.
2) This fouling study further investigated the water flux and water recovery.

Accomplishments

1) Greater than >90% water recovery was achieved and water flux reproducibility was confirmed [100% accomplished].
2) SEM images of the membrane feed and distillate surfaces and cross-sections were collected [100% accomplished].
3) The chemical composition of membrane foulants was analyzed using EDS [100% accomplished].
4) Reviewed the economic information for existing MD processes [100% accomplished].

A4. Test best PP membrane employing realistic AMD in batch MD; Set up open-loop continuous MD; Initiate economic analysis of MD processes.

The three fouled membranes, namely 0.45 micron PTFE from GE Osmonics (QP909), 0.45 micron PTFE from Pall Corporation, and 0.45 micron PP membrane from 3M/Cuno company reported in *Thrust A3* were analyzed by EDS for the presence of Na, a major cation present in the feed used in the accelerated fouling studies. The atomic Na/S ratios were calculated from the EDS data and compared to the Fe/S ratios across the membrane to understand the chemical nature of the foulants. The typical Na/S ratio for the Na sulfate in the feed solution is 2, while the Fe/S ratio is 1.

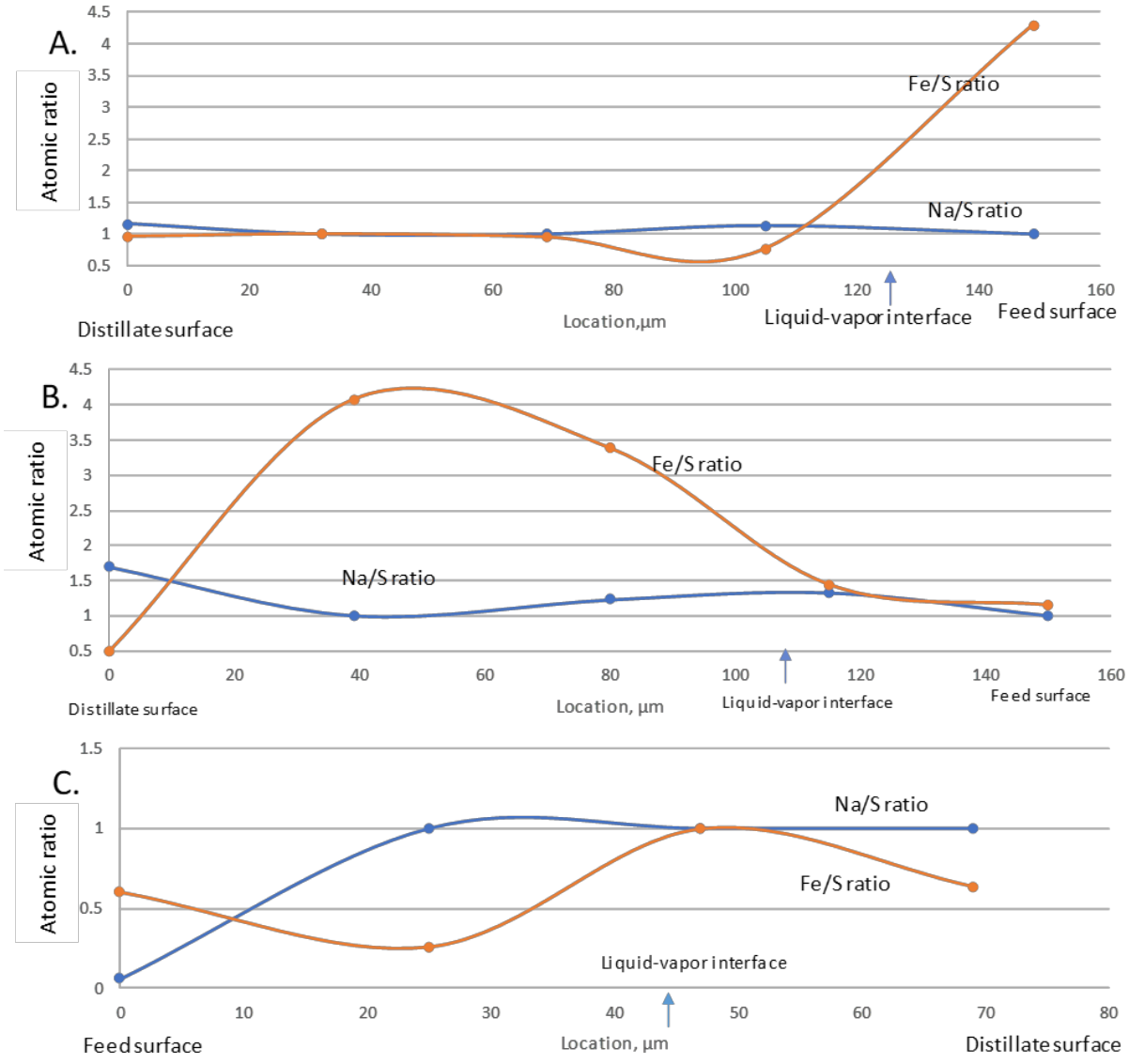

Figure 15. The ratio of Na/S and Fe/S with distance across the cross-section of A) GE PTFE membrane, B) Pall PTFE membrane and C) PP membrane.

Figure 15 shows the Na/S and Fe/S ratios determined for different locations inside the 3 fouled membranes. The Na/S ratios (~1) was relatively constant across the membrane, but were lower than this ratio for Na sulfate indicating that excess sulfate was associated with the presence of Fe. Fouling was accompanied by the accumulation of Fe inside the membrane which was more enhanced (relative to S) for the two PTFE membranes as compared to the PP membrane.

The high Fe/S ratios >1 and low Na/S ratios <2 observed at certain locations inside the membranes were interpreted as locations of the liquid-vapor interface, which also suggested that the fouling was associated with Fe^{2+} oxidation and formation of sulfate-depleted Fmembranes reported previously.

It was observed previously that the three membranes typically functioned for ~18-20 hours without experiencing a noticeable decline in water flux or showing elevated TDS in the distillate when very high initial AMD concentration (46,000 mg/l) was used in batch tests that further concentrated it to ~460 g/l at 90% water recovery. This highly concentrated feed (46,000 mg/l) was replaced with feeds containing realistic AMD compositions. Three of the five compositions reported in *Thrust A3* were repeatedly tested employing the best PP membrane.

Table 17. Realistic AMD compositions tested.

	Location	**Iron, Fe(II) (mg/l)**	**Sulfate, SO_4^{2-} (mg/l)**	**TDS (mg/l)**	**Reference**
Real AMD Compositions in Appalachian Region	Brubacker run, PA	114	381	560	Larson et al. 2014
	Summerlee, WV	275	547	877	
	Upper run, PA	383	903	1,500	
Simulated AMD	-	5,000	30,000	45,000	Previously tested

Table 17 shows the three realistic AMD compositions that had the natural pH of 4.26 and were tested in a batch mode employing the PP membrane. The toxic species (0.2 mg/l Cr, 0.2 mg/l Zn, 0.1 mg/l Se, 0.1 mg/l As, and 0.05 mg/l Cd) were added according to the composition described previously. The water flux was tested for the optimal operating conditions (Condition 1 reported in Table 12), where the heater temperature was set at 90 ℃ and the chiller temperature was at 10 ℃, while the flow rates of the feed and distillate streams were each 30 l/h.

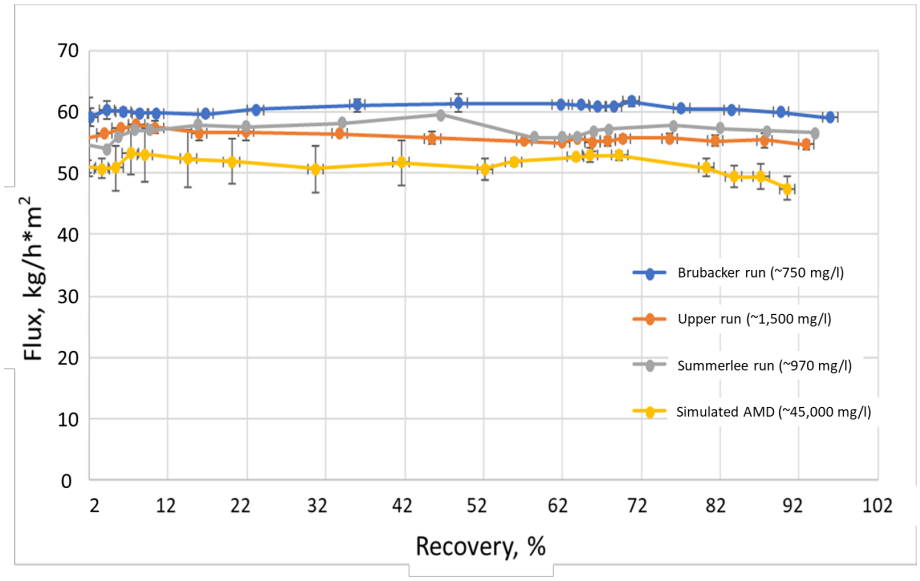

Figure 16. Water flux vs. % water recovery for the 3 realistic AMD compositions and highly concentrated simulated AMD employed to date.

From Figure 16, it can be seen that the water flux for the realistic AMD compositions was ~9-13% higher than the water flux reported previously for the highly concentrated simulated AMD (e.g., Figure 10). It can also be observed that the water flux at >70% water recovery did not decrease to the same extent for the realistic AMD feeds as it did for the highly concentrated AMD feed. Greater than 90% water recovery was achieved in repeated tests, which also confirmed excellent water flux reproducibility over a period of ~58 hours in operation. The PP membrane was removed from the permeation cell when the distillate displayed 40 mg/l of TDS and analyzed by SEM and EDS to characterize fouling.

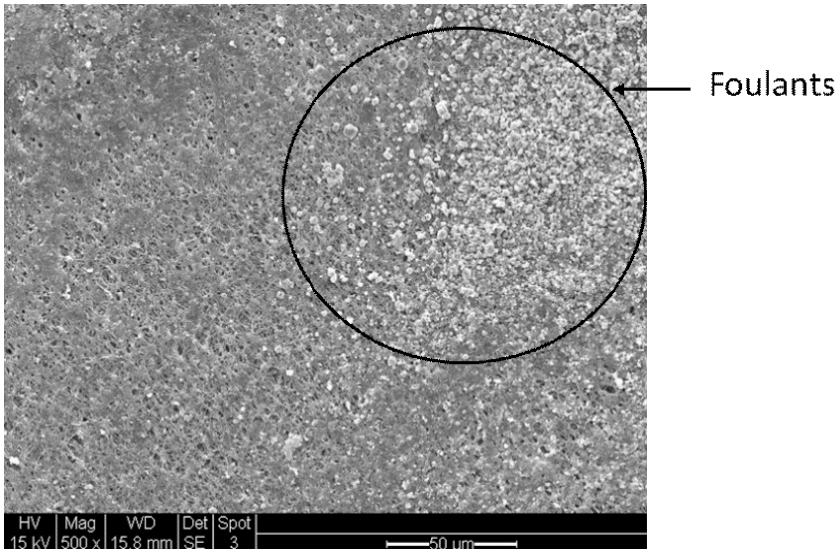

Figure 17. The SEM image of the used PP membrane, at 500x magnification, shows the presence of foulants on the feed surface.

Figure 17 shows noticeable accumulation of foulants on the membrane surface after ~58 hours of operation. An EDS point analysis of the membrane feed and distillate surfaces showed a sharp gradient of Fe concentration that decreased from ~13 at. (atomic) % at the feed surface to ~0.13 at. % at the distillate surface. An EDS line scan was performed for the membrane cross-section shown in Figure 18 to further characterize fouling.

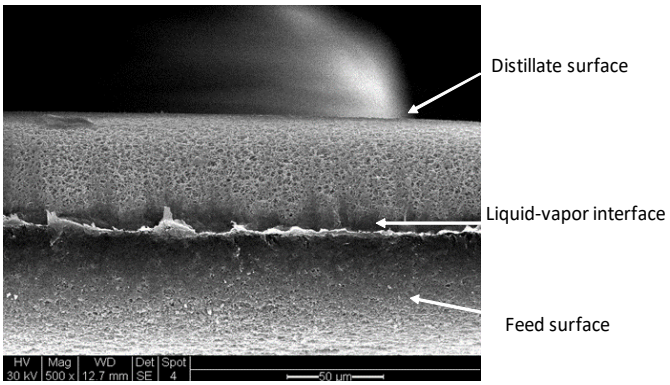

Figure 18. The cross-section of the used PP membrane.

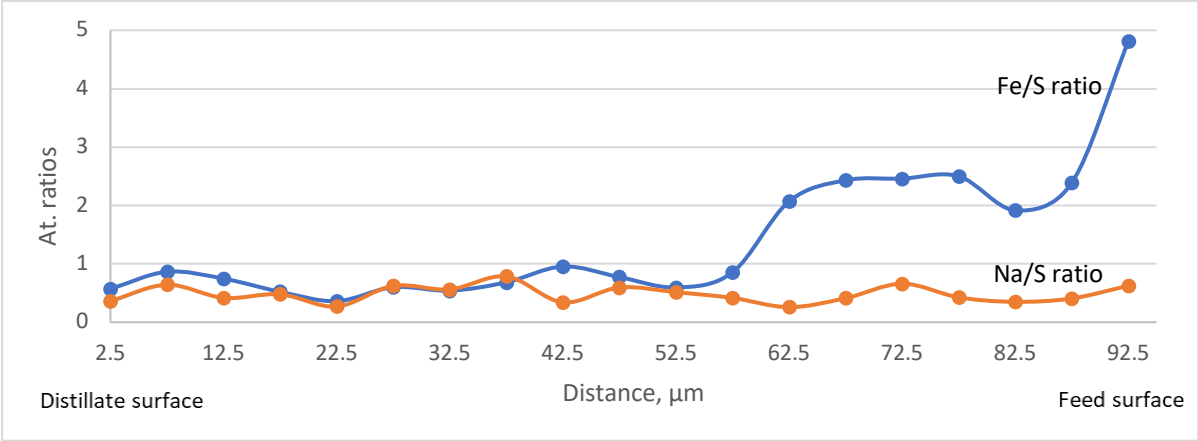

Figure 19. The Na/S and Fe/S ratios calculated from the EDS line scan data.

The surface scans detected the presence of Na, Fe, and S. Therefore, the line scans were used to primarily investigate the presence of these three elements in the membrane cross-section. The EDS data obtained were converted to Na/S and Fe/S atomic ratios. The low Na/S and high Fe/S ratios observed at the feed surface indicated that iron was deposited at the feed surface and inside the active layer (facing the feed) without significant association with sulfate. The cross-sectional analysis indicates that Fe/S ratios decreased from the feed surface to some location ~40 micron below the feed surface in the active layer, which was interpreted as the location of the liquid-vapor interface (Figure 19).

Based upon discussions with Office of Surface Mining Reclamation and Enforcement (OSMRE), it was decided to test a specific Raccoon Creek composition using the best PP membrane. Raccoon Creek is a 114-mile-long (183 km) stream that drains parts of five

Southern Ohio counties. It originates in Hocking County, Ohio, and flows through Vinton County and Gallia County and a corner of Meigs County. Its largest tributary, Little Raccoon Creek, arises in Jackson County. The watershed also includes part of Athens County, drained by another tributary, Hewett Fork. The other major tributaries are Elk Fork, located entirely in Vinton County, and Brushy Fork, which is mostly in Vinton County with a small area in Hocking County.

Table 18. Raccoon Creek AMD composition on 8/22/99.

Site	TDS, mg/l	SO_4^{2-}, mg/l	Fe, mg/l	Mn, mg/l	Al, mg/l	pH
FR0126	7,900	4,346	1,417	29	171	2.4

Table 18 shows the stream composition of a specific site (FR0126) in the Raccoon Creek. This composition was prepared in our lab meeting all parameters shown in Table 18 and tested using the 0.45-micron PP membrane. A fresh PP membrane was placed inside the permeation cell and the water flux was measured in batch tests conducted for Condition 1 reported in Table 11 corresponding to $\Delta T = 60$ °C and the feed/distillate flow rates of 30 l/h.

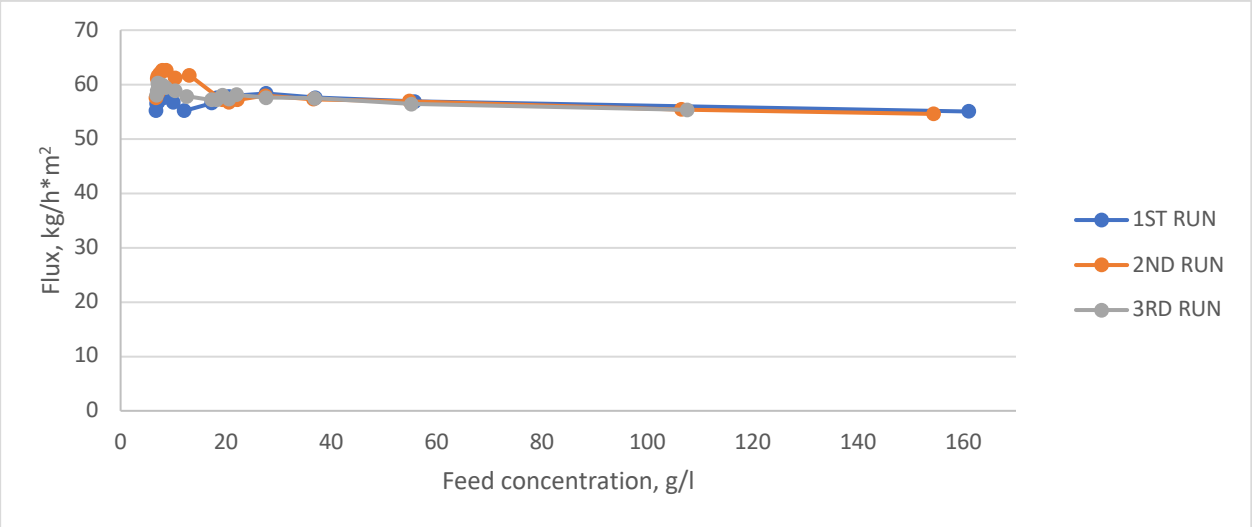

Figure 20. Water flux vs. feed concentration for the Raccoon Creek AMD composition (site FR0126).

Figure 20 shows that the water flux was very similar to that obtained using the realistic compositions shown in Figure 16, although the TDS content in the Raccoon Creek was ~6 times higher (Tables 17 and 18).

Economics:

The economic analysis was conducted by carrying out the steady-state mass and energy

balances using PROII simulation software. There were 6 steps in carrying out a PROII simulation:

1) Build the Process Flow Diagram (PFD) or select the necessary unit operations, e.g., distillation columns, heat exchangers, pressure change columns, etc.
2) Select the chemical components present in the stream from a built-in database or enter them manually.
3) Select the thermodynamic model to calculate entropies, enthalpies, and transport properties.
4) Provide stream properties, such as the chemical compositions, flowrates, temperatures, pressures, etc.
5) Provide the unit operator data, e.g., outlet temperature of heat exchanger or reflux ratio for a column, etc.
6) Finally, simulate the operation and troubleshoot any errors.

Example: Simulating a simple heat exchanger

Figure 21 shows a simple heat exchanger chosen as the unit operator from the PFD palette on the right of the screen. The simple heat exchanger was used to simulate the chiller used in the batch MD process. The components of the input stream were selected or manually defined by selecting the *Component Selection* button on the menu bar. The appropriate thermodynamic model was selected by clicking on the *Thermo* button on menu bar. The input and output streams were then added to the heat exchanger.

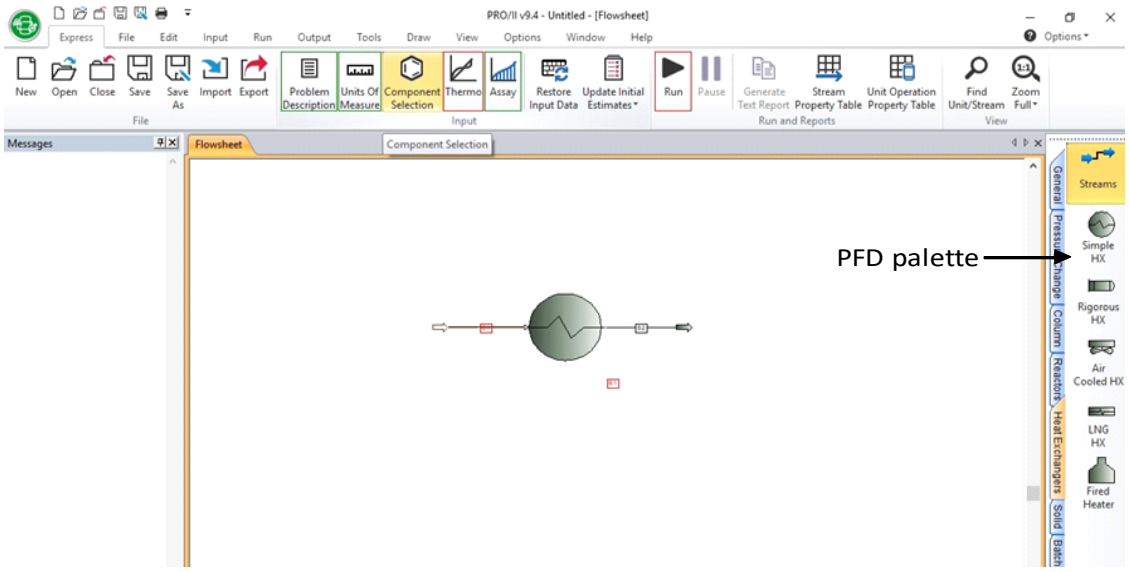

Figure 21. Simulation of a simple heat exchanger.

Figure 22 shows the dialog boxes needed to define the input stream parameters: flowrate, composition, and thermal conditions. These data can be entered by clicking on the input stream to the heat exchanger, shown in Figure 21**.** The conditions for the process unit can be entered by clicking on the heat exchanger, e.g., specifications of the hot process stream, the cold utility

stream, etc. The simulation was executed by clicking on the *Run* button on the toolbar (seen in Figure 21) after troubleshooting the errors.

Simulation results

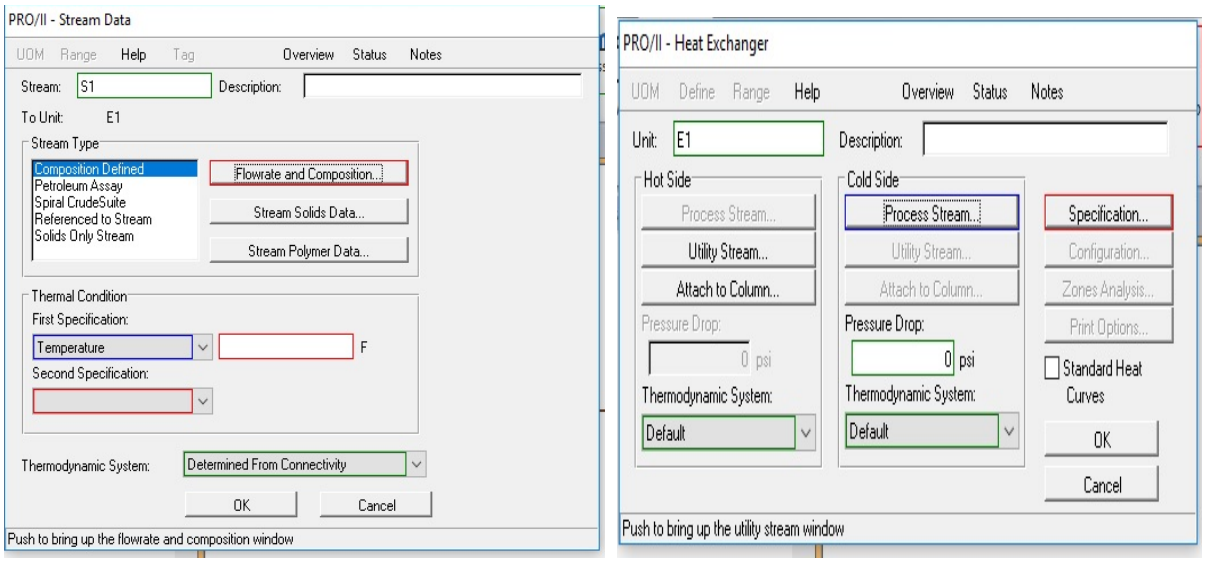

Figure 22. Stream data specification (left) and heat exchanger specification (right) dialog boxes.

E1 is the simple heat exchanger (Hx) simulated. Table 19 shows the results of the simulation. The duty of the heat exchanger is defined as the amount of energy transferred to the chiller per unit time to cool down the input water stream. This was evaluated to be 0.001 x 10^6 kJ/h or 0.30kW. This is the amount of energy required to lower the temperature of 30 l/h of water used in the current batch MD process. LMTD is the logarithmic mean temperature difference which serves as the driving force for the heat transfer between the hot incoming water and the cold utility water. 9.4418 K was the LMTD of the chiller used. The hot product temperature and the cold product temperatures are enetered manually while defining the streams and the unit operator.

Table 19. Data results from simulation.

Simple HX - 'E1'		
Property	**Value**	**Units**
Hx Name	E1	
Hx Description		
Duty	0.001	x 10^6 kJ/h
LMTD	9.4418	K
Hot Prod Temp	289	K
Cold Prod Temp	283	K

This example shows how a standalone component, such as the chiller, pumps, the heater, etc., can be simulated using PROII. The simulation procedure is more challenging to set up for the entire MD process where mass and energy balances have to be taken into account. The mass balance for the individual cations in real process samples will be determined with the help of ICP-MS elemental analysis, while the energy balances will be determined from the inlet/outlet

temperatures, volumetric rate measurements, etc., for all process streams. The mass and energy balances will be set up based on the experimental data from the open-loop continuous processes. Therefore, the economic evaluation of the MD process is expected to be completed at the end of the project period after all the experimental data becomes available.

Significant Events

1. Investigated the presence of Na in 3 fouled membranes: 0.45-micron polypropylene (PP) from 3M/Cuno Company; 0.45 micron polytetrafluoroethylene (PTFE) from GE Osmonics (QP909); and a new 0.45-micron PTFE membrane (PTF045DL0A) from Pall Corporation, that underwent accelerated fouling as described in *Thrust A3*.
2. Conducted batch-mode testing of the best membrane (0.45 micron PP membrane from 3M/Cuno Company) employing realistic AMD feed compositions described in the literature and reported previously.
3. Completed setup of a new open-loop continuous-mode MD system.
4. Further tested the best PP membrane employing simulated Raccoon Creek AMD compositions in a batch mode.
5. Initiated economic analysis of the components in the MD system.

Accomplishments

1. The Na presence in the 3 membranes was characterized by EDS. [100% accomplished].
2. The effects of realistic AMD concentrations and acidity on the water flux and membrane durability were studied for the best PP membrane. [100% accomplished].
3. The best PP membrane was tested in a batch mode employing the Raccoon Creek FR0126 site composition [100% accomplished].
4. Accomplished >90% water recovery and excellent water flux reproducibility (± 2 %) for the Raccoon Creek FR0126 site composition [100% accomplished].
5. Made significant progress in setting up economic analysis of the MD process [40% accomplished].

B1. Conduct open-loop continuous (OLC) MD of simulated Raccoon Creek AMD (OSMRE site FR0126); Characterize fouling of used membranes; Study energy requirements of OLC MD

0.45-micron polypropylene membrane (PP) was identified to be the best membrane in previous thrusts. This PP membrane was employed in the open-loop continuous mode to test simulated Raccoon Creek AMD as feed. The simulated Raccoon Creek AMD feed had a TDS content of ~9.8 g/l. In open-loop continuous MD mode, pure water was added to the feed at the same rate as it was removed by the MD process while maintaining the feed at concentration corresponding to ~90% water recovery (TDS ~ 98 g/l) as shown in Figure 23.

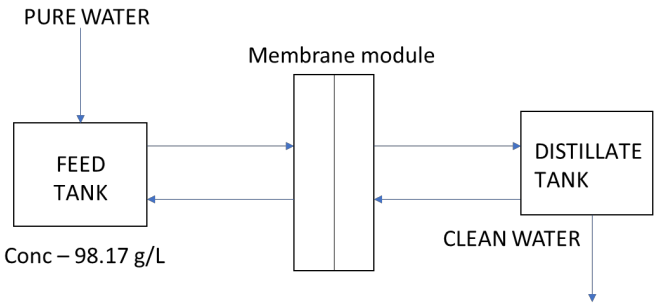

Figure 23. The schematic of the open-loop continuous MD.

The open-loop continuous MD process was run under the best operating conditions with a ΔT of 60 °C and feed/distillate flow rates of 30 l/h. Unlike the batch mode, this open-loop MD process involved testing the water flux using the simulated Raccoon Creek feed at very high TDS concentrations on a continuous basis.

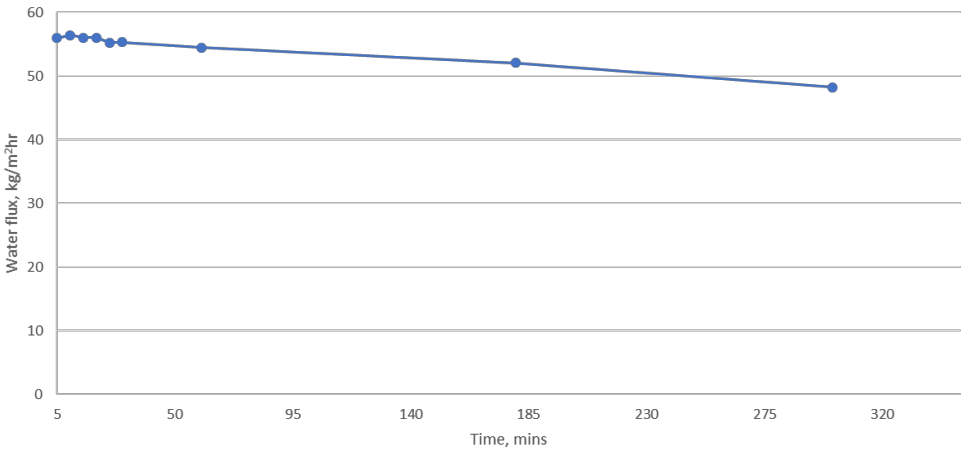

Figure 24. Water flux vs. time in the open-loop continuous MD process employing simulated Raccoon Creek water as feed.

Figure 24 shows a gradual ~15% reduction in the water flux after 5 hours (300 minutes) of operation in the open-loop continuous mode employing simulated Raccoon Creek water as feed. The MD process was then stopped, and the system was washed with low pH water to clean the membrane. Although the membrane performance was restored, the water flux declined again after ~4 hours. This reduction in the water flux suggested membrane fouling and scaling as the membrane was exposed to feeds with very high TDS concentrations corresponding to 90% water recovery shown in Table 20.

Table 20. The element concentrations in simulated Raccoon Creek feed corresponding to 90% water recovery based on information provided by OSMRE.

Element	Fe(II)*	Sulfate	Na	Al	Mn	TDS
Conc, g/l	14.17	43.46	38.54	1.710	0.290	98.17

* Fe(II) was used to prepare this feed

The membrane was removed for characterization of the foulants by SEM and EDS. The presence of fouling and scaling was apparent as the membrane was discolored.

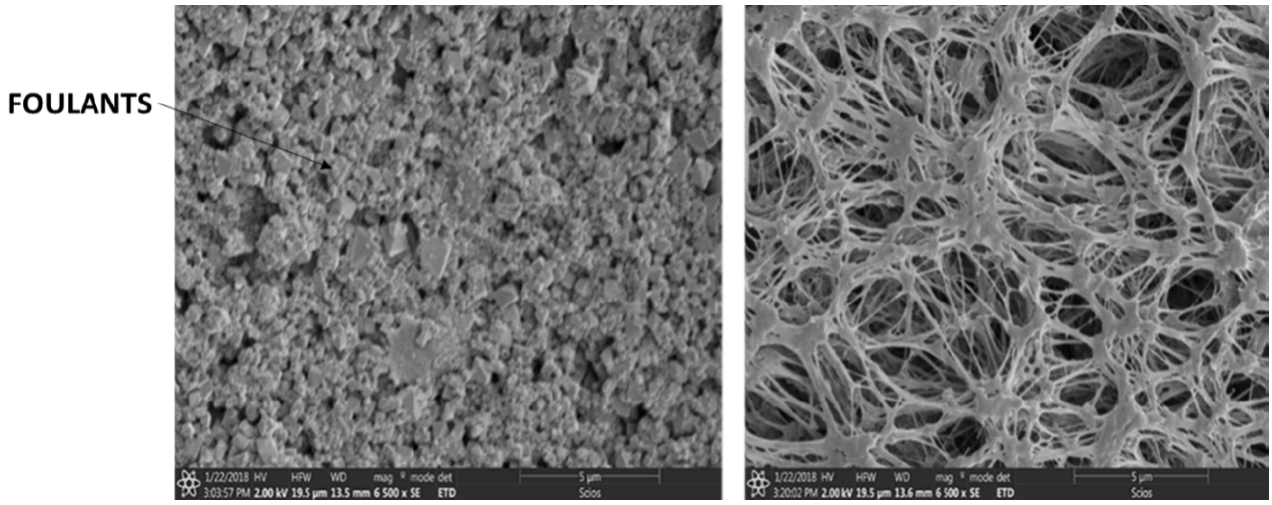

Figure 25. The feed (left) and distillate (right) surfaces of the used PP membrane at 6500x magnification.

The fresh PP membrane has the same fibrous structure on both the feed and distillate surfaces. However, it can be seen from Figure 25 that a layer of ~3 μm foulant particles is present on the feed surface of the used membrane. It can also be seen that the distillate surface was clean which is suggested by its fibrous structure. A quantitative EDS elemental analysis was done on the two surfaces for two small membrane areas at 8,000x magnification. The EDS analysis confirmed that the distillate surface was clean as only carbon was detected.

Table 21. The major element concentrations (at. %) at the feed surface of the fouled PP membrane and in the feed solution.

Element	at. % on feed surface	at. % in feed solution
Na	10	24
S	36	41
Fe	46	23
Al	8	12

Table 21 shows the EDS atomic percentages of the major elements present on the feed surface of the membrane after it was fouled during the open-loop continuous MD process employing simulated Raccoon Creek water as feed. To provide a better understanding of membrane fouling, the concentrations of the major elements present on the membrane feed surface were compared to their concentrations in the simulated feed solution. The atomic percentages of the major elements in the feed solution was calculated by taking the dry weight of the salts added in water to make up the simulated feed. A significant enhancement of Fe concentration and depletion of S is visible on the feed surface suggesting that the membrane fouling is associated with deposition of some Fe (oxy)hydroxide phase. Since the simulated feed has Fe, S and Na as the major elements, a comparison of the atomic ratio of iron to sulfur in the feed solution and on the feed surface of the membrane can aid in understanding the composition of the membrane foulants (Table 22). The high Fe/S ratio on the feed surface of the used membrane indicated that Fe is significantly enriched in the foulant particles as compared to the feed solution. Based on the stoichiometry of both Fe(II) and Fe(III) sulfates (Fe/S of 1 and 0.67, respectively), the S content in the foulant is highly insufficient to balance the cation charge suggesting that it is balanced by oxygen due to hydrolysis and/or oxidation of the original Fe(II) used to make this simulated feed. Moreover, we believe that the membrane fouling

occurred in these MD tests because we used a highly concentrated feed solution of Fe(II) sulfate that underwent oxidation under MD conditions resulting in fouling.

Table 22. Atomic ratios of the foulant elements present on the feed surface of the used PP membrane.

Atomic Ratio	Feed solution	Membrane feed surface
Fe/S	0.56	1.27 (2.42*)
Na/S	0.57	0.25

*This Fe/S ratio was estimated by subtracting the sulfur associated with Al and Na cations in the foulant according to the stoichiometry of Al and Na sulfates

Real AMD was collected from a site on Raccoon Creek at Carbondale doser in Nelsonville, Ohio. The GPS coordinates of the site are N 39° 22' 46.66", W 82° 16' 01.86". This acid mine discharge was collected before treatment with calcium oxide and stored in plastic containers in a freezer. The parameters that define the water quality were determined by both qualitative and quantitative analysis. Physical parameters, such as total suspended solids (TSS), total dissolved solids (TDS), and pH of the water were measured. The TSS is defined as the dry weight of the particles trapped by a filter that separated the particles from the water. A glass fiber filter from Advantec with pores sized 0.4 μm was used to filter the Raccoon Creek water. The filter was weighed prior to filtering the creek water, used to separate suspended solids, and then dried overnight in an oven at 80 ℃. The dried filter containing suspended solids was weighed and the TSS content (mg/l) was then calculated as follows:

$$TSS, \frac{mg}{L} = \frac{wt\ of\ filter\ (pre), mg - wt\ of\ filter(post), mg}{vol\ of\ water\ filtered, L}$$

The TSS content in the creek water was determined to be ~70 mg/l , while the TDS content was measured to be 900 mg/l, and the pH of the water was 3.20. It is important to note that this TDS content is much lower than ~9.8 g/l value for the simulated creek water (10% of the total value in the last column in Table 20). The glass fiber filter that was used to filter the creek water was then characterized by SEM and EDS to understand the chemical composition of the suspended solids in the water.

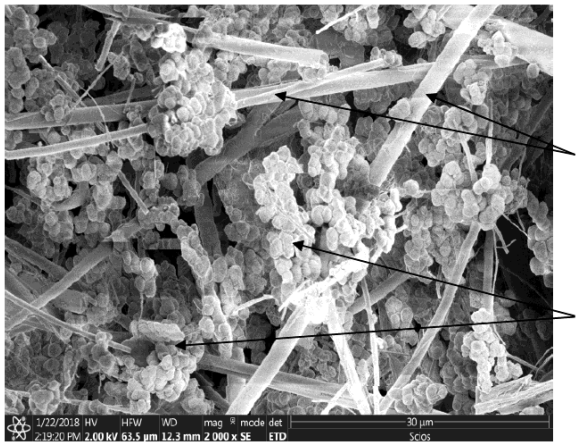

Element	at. % (TSS)
Fe	73.30
Na	14.14
S	12.56

Atomic ratio

Fe/S	5.83

Figure 26. SEM image of the glass fiber filter used to filter the creek water at 2000x maginification (left) and the EDS analysis of suspended solids retained by this filter, at. % (top) and atomic ratio (bottom).

Figure 26 shows the SEM image of the glass fiber filter. The suspended particles can be seen clearly in this image. To better characterize the chemical composition of the TSS particles retained by the filter, we calculated the Fe/S ratio from the at. % data obtained shown in Figure 26. The oxidation of pyrite (FeS_2) is the major contributor to acid mine drainage which initially forms dissolved iron sulfate. The high Fe/S ratio (~5.83) observed for TSS particles indicated that iron was converted into S-depleted (oxy)hydroxide phase under aerobic conditions. An X-ray diffraction (XRD) analysis of these particles retained by the filter will be done in the near future to probe the nature of this iron oxide phase.

The chemical composition of the creek water was qualitatively analyzed by inductively coupled plasma mass spectrometry (ICP-MS). This analysis was done on an unfiltered creek water sample, where the suspended solids were dissolved using 2 weight % (wt.%) nitric acid prior to analysis. The creek water was diluted from a TDS concentration of 900 mg/l to ~100 µg/l using 2 wt.% nitric acid. The major elements of interest (Table 23) were initially chosen for analysis based on the chemical compositions of the Raccoon Creek water recommended by Dr. Beckford and Sara Kreitzer, U.S Office of Surface Mining Reclamation and Enforcement (OSMRE) Hydrologists. It should be noted that the combined concentration of Fe, Mn, Al and Mg in the creek water corresponded to ~90% (790 mg/l) of the total dissolved solids content of 900 mg/l. Based on this preliminary ICP-MS analysis, it should be noted that the current Raccoon Creek water composition is very different from the composition of the simulated Raccoon Creek AMD previously used as feed.

Table 23. ICP-MS analysis of major elements present in Raccoon Creek water.

Element	Concentration, mg/l
Fe	168
Mn	10.4
Al	9
Mg	600

As indicated above, the oxidation state of Fe present in the creek water is expected to be highly important for the membrane fouling behavior during MD process. If nearly all Fe is present as Fe(III), very little fouling is expected for this oxidation state of Fe, whereas high Fe(II) concentrations are expected to result in fouling due to its oxidation and precipitation as an oxide phase. Therefore, we conducted quantitative analysis of Fe(II) and Fe(III) present

in the creek water by UV-visible spectrophotometry (3500-Fe-B Phenanthroline method). Briefly, this method involves the following steps:

Principle: Iron in +2 oxidation state reacts with 1,10–phenanthroline, a ligand, to give an orange-red colored complex which absorbs ultraviolet light with maximum absorbance at 510 nm. The creek water was analyzed for total iron, ferrous and ferric concentrations.

Total Iron: A small sample of the creek water was acidified to dissolve all the iron. This acidified sample was then diluted and all the iron in the sample was reduced to Fe(II) with hydroxylamine hydrochloride solution. This sample was then mixed with phenanthroline solution to form the colored complex.

Ferrous iron: The acidified sample of the creek water was diluted and an appropriate volume of phenanthroline solution was added to form the colored complex. This analysis does not involve the addition of hydroxylamine hydrochloride.

Ferric iron: The Fe(III) concentration was determined by subtracting the concentration of ferrous iron from total iron.

This analysis showed that ~70% of all iron is present in the creek water as Fe(III). It also indicates that all simulated AMD compositions tested in the batch MD mode and reported in *Thrusts A1-A4* likely had very high Fe(II) concentrations, making it more susceptible to oxidation and precipitation inside the membrane as foulant particles. Moreover, Fe(II) is present at ~30 times lower concentration in the real creek water as compared to simulated creek water (30% of 168 mg/l or ~50 mg/l vs. 1,417 mg/l for the simulated creek water). It should be further noted that the Fe concentration determined by ICP-MS also includes a contribution from suspended solids which were dissolved by dilute nitric acid prior to analysis, while suspended solids will be removed from the creek water by filtration prior to MD. The true Fe(II) concentration in filtered creek water is expected to be lower than 50 mg/l. Therefore, the membrane is expected to experience much less significant fouling when using filtered real creek water as the feed.

Process Economics:

Economic analysis was conducted by carrying out the steady-state mass and energy balances using PROII simulation software. There are 6 steps in carrying out a PROII simulation:

1) Build the Process Flow Diagram (PFD) or select the necessary unit operations, e.g., distillation columns, heat exchangers, pressure change columns, etc.
2) Select the chemical components present in the stream from a built-in database or enter them manually.
3) Select the thermodynamic model to calculate entropies, enthalpies, and transport properties.
4) Provide stream properties, such as the chemical compositions, flowrates, temperatures, pressures, etc.
5) Provide the unit operator data, e.g., outlet temperature of heat exchanger or reflux ratio for a column, etc.
6) Finally, simulate the operation and troubleshoot any errors.

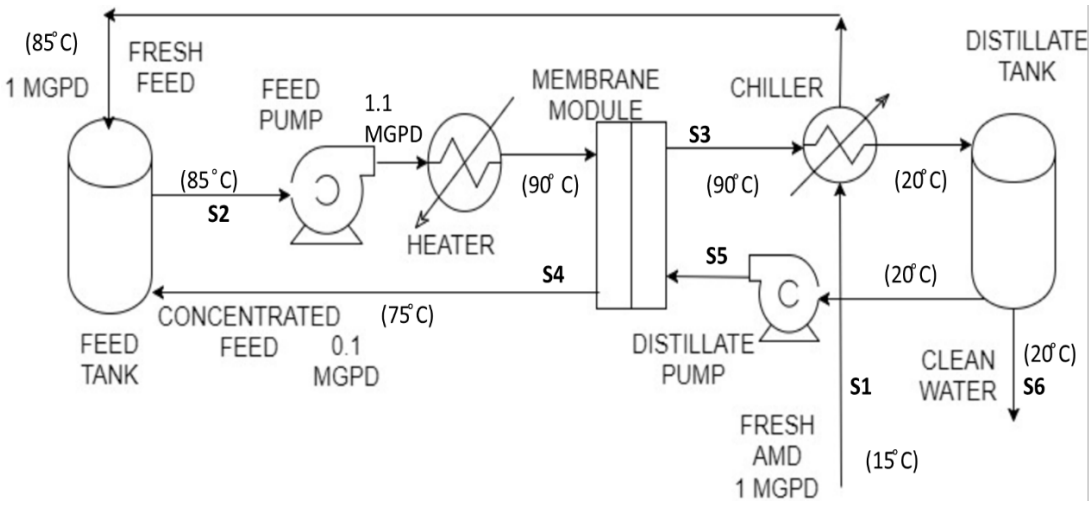

Figure 27. The PFD of the open-loop continuous MD process.

Figure 27 shows the process flow diagram (PFD) of the open-loop continuous MD process. The PFD shows that fresh AMD at 15 ℃ (S1) will be continuously fed to the feed tank from which it is pumped to the membrane after being heated to ~85 ℃ (S2). The concentrated feed from the module (S4) is recycled back to the feed tank. The clean water recovered (S3) in the distillation process is pumped to the distillate tank from which the water is recycled at low temperatures (S5) to the membrane surface to provide the temperature gradient between the hot feed and cold distillate across the membrane surfaces. The total flowrate of AMD treated by the membrane module will be ~1.1 MGPD of which 90% will be recovered as pure water (S6). The remaining 0.1 MGPD of the concentrated feed (S4) will be sent back to the feed tank to mix with the incoming 1 MGPD of fresh feed. This process flow diagram will be simulated with the mass balances set up. The energy requirements solely depend on the inlet/outlet temperatures and the volumetric flow rates of the streams. These energy requirements represent the cost of treating 1 million gallons per day of acid mine drainage in an open-loop continuous process (Table 24).

These MD energy requirements correspond to daily costs of circa (ca.) $1,690 obtained using the industrial electricity price of $0.0668/kWh reported for Ohio in November 2017 by the US Energy Information Administration (USEIA 2017). The mass balances for this simulation will be set up based on the experimental data obtained after further work on the open-loop continuous MD process. Once the mass balance is set up, the simulation will be done again. The composition of the streams, metal concentrations etc. will be presented along with the energy requirements of the completed MD process.

Table 24. Preliminary energy requirements for a 1 million gallons of AMD/day (GPD) MD process.

Heating requirement: Assuming fresh AMD feed at 1 MGPD (S1) and the recycled 0.1 MGPD concentrated feed (S4) enter the heater at 80 °C. Heater utilizing water at 90 °C as a medium to heat the feed at 85 °C to 90 °C.	1.024 MW
Cooling requirement: Assuming 90% of the total flowrate recovered from the membrane (S3) exchanges heat with fresh AMD at 15°C (S1) MD distillate from 90 to 20 °C (fresh AMD is raised from 15 to 85 °C)	0 (11.968) MW
Pumping requirement: 1) To pump the mixed AMD stream (S2) using a pump with 82% efficiency 2) To pump the clean distillate water out of the system (S6)	0.030 MW
Total	**1.054 MW**

Significant Events

1) The best membrane identified previously, i.e., 0.45-micron polypropylene (PP) from 3M/Cuno Company, was tested in the open-loop continuous mode under the best operating conditions using simulated AMD feed.
2) The used PP membrane was characterized by SEM and EDS to investigate fouling and scaling.
3) Real Raccoon Creek AMD water (creek water) was collected from Carbondale doser site to be tested as feed in the open-loop continuous mode.
4) The creek water collected was qualitatively and quantitatively analyzed.
5) The energy requirements of the open-loop continuous MD process were studied.

Accomplishments

1) PP membrane was tested in the open-loop continuous mode using simulated Raccoon Creek AMD feed under the best MD conditions [100% accomplished].
2) The effect of high simulated AMD concentration at 90% water recovery on the water flux was studied [100% accomplished].
3) The PP membrane was characterized by SEM and EDS to investigate fouling and scaling [100% accomplished].
4) The real Raccoon Creek water collected was analyzed to understand the chemical composition by qualitative and quantitative methods [100% accomplished].
5) Energy requirements of treating 1 million gallons per day of simulated Raccoon Creek water were estimated by process simulations using PRO/II software [100 % accomplished].

B2. Employ real Raccoon Creek AMD in batch MD and recover ~90% water; Characterize fouling of used membranes

0.45 µm pore polypropylene membrane (PP) identified previously as the best membrane was employed in the batch MD using real Raccoon Creek AMD collected from a site on Carbondale doser in Nelsonville, Ohio as feed. The real Raccoon Creek AMD feed collected was

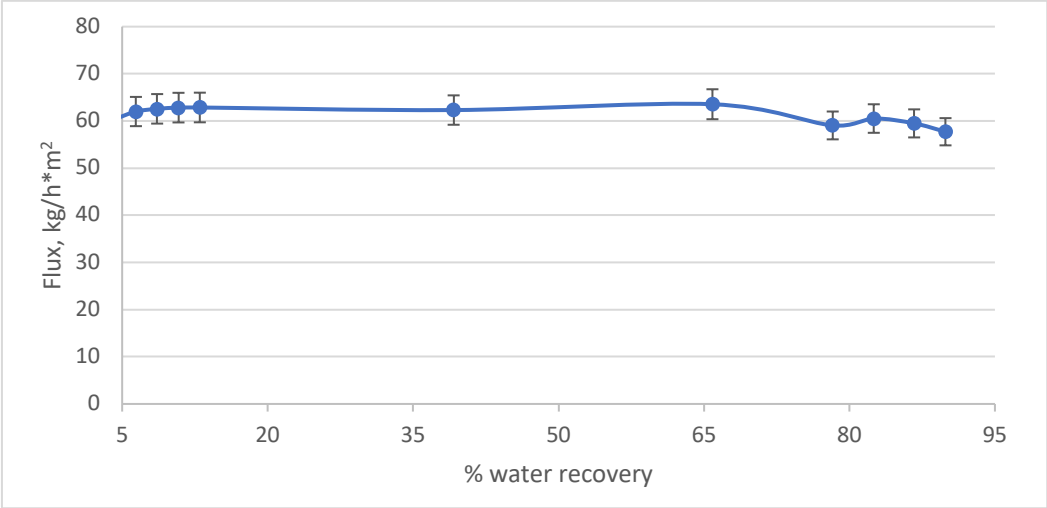

Figure 28. Water flux vs. water recovery for fresh creek water in batch MD mode.

stored frozen in plastic containers, melted as needed, filtered, and used fresh as MD feed. The pH of the freshly thawed and filtered creek water was 2.80 and its TDS content was 730 mg/l. The MD tests were conducted with the feed (creek water, CW) heated to 90 ℃ and the distillate cooled to 20 ℃ with the respective flow rates at ~30 l/h.

As Figure 28 indicates, 90% of water can be recovered from fresh creek water (Day 1) without an appreciable decline in the water flux. CW was then stored in a refrigerator at 3 ℃ for up to 60 days and its pH and TDS were monitored regularly prior to MD experiments. It should be noted that this CW was apparently saturated with respect to gypsum dissolved at 3 ℃ because excess gypsum (previously identified by XRD) was visible at the bottom of the CW container. The data shown in Table 25 demonstrated that the pH and TDS of CW increased rapidly over first several days of storing it at room temperature, which suggested CW ageing. Furthermore, it was observed that as this creek water aged, the MD water flux decreased significantly at high water recovery greater than 75% (Figure 29). The MD system was washed with dilute sulfuric acid after every run where

Table 25. pH and TDS content of the creek water as a function of time stored at 3 ℃.

Time, days	pH	TDS, mg/l
1	2.80	730
2	3.30	740
3	3.53	760
4	4.30	850
5	4.44	900

aged CW was used to remove the foulants and recover the membrane performance.

However, the TDS content and pH of the CW stopped changing after 5 days of its storage at 3 ℃. To better characterize the chemical composition of the aged creek water, a small volume of filtered aged water containing TDS ~900 mg/l after ~20 days of storage was evaporated in a

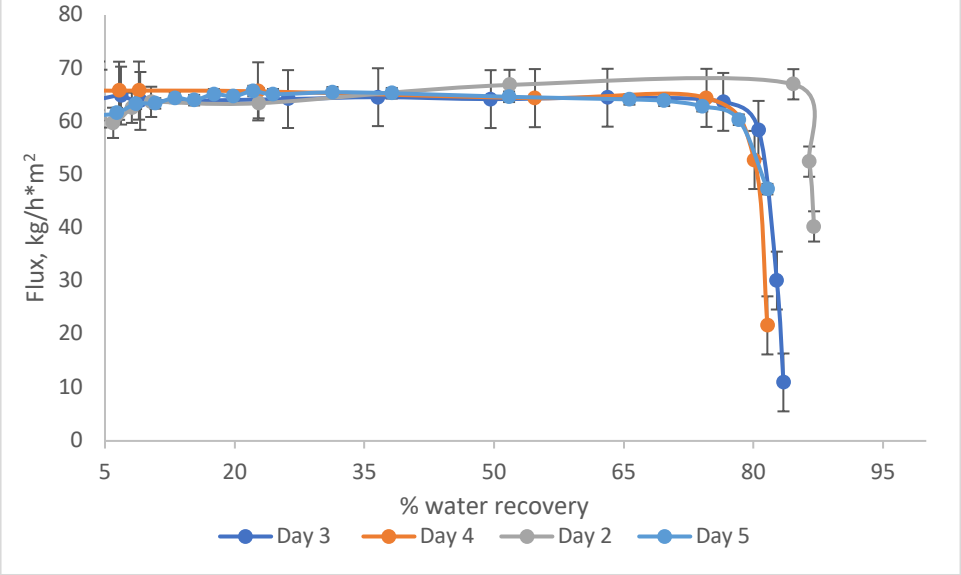

Figure 29. Water flux vs. water recovery for aged creek water (days 2- 5) in batch MD tests.

fume hood and the solid residue investigated by SEM/EDS.

The major element concentrations in the creek water were estimated for the TDS content of 900 mg/l as the basis using the EDS analysis results shown in Figure 30. Since calcium and sulfate predominated in this evaporated solid, we expected it to be composed of calcium sulfate phase(s). The needle-like morphology of the evaporated solid in Figure 30 is representative of gypsum. We also assumed that nearly all sulfate in the aged creek water (483.6 mg/l) will be associated with stoichiometric ~200 mg/l of Ca to form ~864.5 mg/l of dissolved gypsum ($CaSO_4 \cdot 2H_2O$). This analysis indicated that calcium was present in excess to sulfate anions in the aged creek water, possibly as calcite that has a significantly lower solubility in water than gypsum and other hydrated calcium sulfate phases. Based on the dissolved gypsum concentration of ~864.5 mg/l in the aged CW at 3 ℃ and the gypsum solubility of ~1.73 g/l in water at 90 ℃, we estimated that gypsum becomes saturated in concentrated aged CW at 90 ℃ when the water recovery reaches ~50%. This conclusion is in good agreement with the water

Elements	Atomic %	Weight %	Conc, mg/L
Magnesium	9	6	55.8
Iron	7	11	102.3
Calcium	27	31	288.3
Sulfate	57	52	483.6

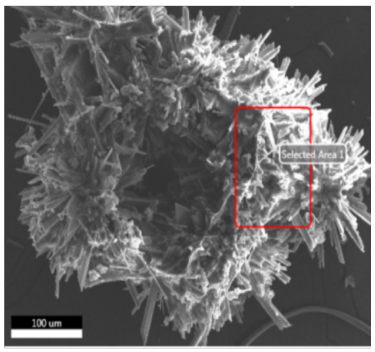

Figure 30. The elemental EDS composition of the evaporated creek water aged for 20 days at 3 ℃ (left) and SEM image of the precipitate.

flux data observed in the batch MD tests employing aged CW which show the flux declining rapidly after reaching ~75% water recovery (Figure 29).

The used and fouled PP membrane after these MD tests was investigated by SEM and EDS for presence of scaling and fouling. Figure 31 shows the presence of the same needle-like particles on the surface of the membrane facing the feed as those found in the evaporated aged CW (Figure 30) suggesting gypsum scaling. The point EDS analysis was done on different spots on the membrane surface to confirm the chemical composition of this scalant. This elemental analysis indicated the scalant was made up of Ca and S only. The average atomic percentages of S and Ca were found to be ~46 and ~54% on the membrane surface confirming that the CW becomes saturated with calcium sulfate at greater than 50% water recovery at 90 °C. It should be noted that the calcium content in this scalant was higher than that expected for gypsum alone suggesting the presence of not only gypsum, but also other Ca-containing phase(s) than sulfates. This observation is in agreement with the EDS analysis results for the solid residue of the evaporated aged CW which also indicated an excess of Ca over S (Figure 30). However, it should be emphasized that this fouling behavior during MD was observed only for the aged CW, while 90% water recovery was achieved for freshly thawed and filtered creek water without any evidence of flux decline even at 90% water recovery.

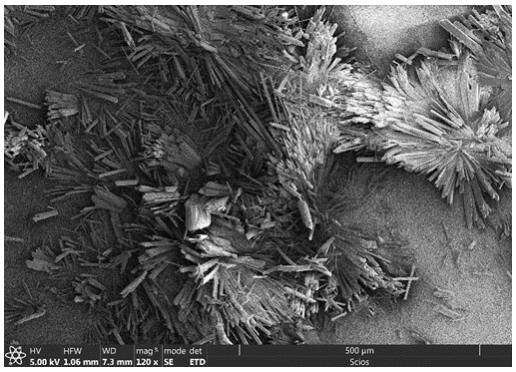

Figure 31. The SEM image of the feed surface of the used PP membrane at 120x magnification showing the presence of foulants.

Lastly, we characterized the suspended solids observed to form in the aged CW (aged for 60 days, TDS ~ 900 mg/l) when the water recovery reached 80% in the batch MD test at 90 °C. This concentrated CW was cooled to room temperature and filtered to remove the observed precipitate. The crystal phases present in this precipitate were detected by powder X-ray diffraction (XRD) using a PANalytical X'pert diffractometer equipped with Cu Kα radiation source. The XRD data were collected in a step scan mode at 2θ=10-70° for a step size of 0.05 °/s, collecting time of 1 s/step, 40 A filament current and 45 kV accelerating voltage.

The XRD patterns (Figure 32) indicated that the precipitate isolated from the concentrated creek water contained gypsum ($CaSO_4 \cdot 2H_2O$), bassinite ($CaSO_4 \cdot 0.5H_2O$), and calcite ($CaCO_3$), further confirming that the concentrated aged CW became supersaturated with these phases after reaching ~50% water recovery at 90 °C, which fouled the membrane and resulted in a significant water flux reduction.

We also investigated the impact of ageing on the Fe^{3+}/Fe^{2+} ratios in CW, since it is well known that the oxidation of Fe^{2+} to Fe^{3+} in solution can be facilitated by atmospheric oxygen, e.g., according to the following half-reaction leading to an increase in solution pH and TDS:

$$Fe^{2+} + 1/2O_2 + H_2O \rightarrow Fe^{3+} + 2OH^- \quad \text{(Eq. 1)}$$

Two samples of CW at pH 3.50 and 4.30 that were aged for 2 and 3 days, respectively (Table 25), were analyzed by UV spectrophotometry as described previously to characterize the speciation of ferrous and ferric iron species. As the data shown in Table 26 indicated, the Fe^{3+}/Fe^{2+} ratio increased with ageing time suggesting that the ferrous iron is oxidized to ferric iron during ageing, which causes a simultaneous increase in the solution pH. Although the Fe^{2+} oxidation by atmospheric oxygen according to Eq. 1 can explain increases in TDS and pH with time, it is not immediately obvious that it may also be relevant for gypsum and calcite fouling of the PP membrane when aged CW is used as MD feed. We believe that increasing CW pH and iron oxidation state with ageing time results in additional dissolution of some precipitated gypsum present in CW stored at 3 °C. This extra gypsum is dissolved to provide sulfate anions to balance increased positive charge of iron cations due to Fe^{2+} oxidation by air (Fe^{2+} → Fe^{3+}), while additional dissolved Ca^{2+} cations balance the OH^- anions as suggested by the following equation:

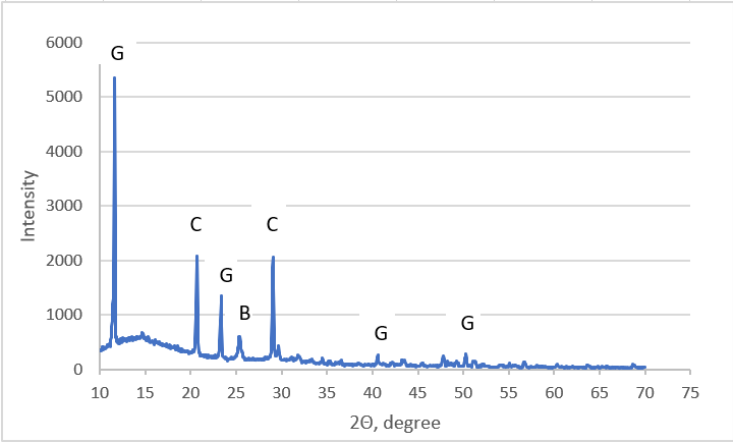

Figure 32. XRD pattern of the precipitate isolated at 80% water recovery from the creek water aged for 60 days and used in batch MD test at 90 °C. G- gypsum (JCPDS 01-070-0982); B – bassinite (JCDPS 00-041-0224) and C – calcite (JCDPS-47-1743) (JCPDS, 1986).

$$2FeSO_4 + 1/2O_2 + H_2O + CaSO_4 \rightarrow Fe_2(SO_4)_3 + Ca(OH)_2 \quad \text{(Eq. 2)}$$

The presence of superstoichiometric Ca in the aged CW (Figure 30) relative to sulfate supports this conclusion. However, calcite is observed in the solids precipitated from the concentrated aged CW (Figure 32) instead of calcium hydroxide indicating that the latter is rapidly converted to highly insoluble calcite by reacting with dissolved atmospheric carbon dioxide. Therefore, the overall chemical transformation of CW with time under ambient conditions which explains all experimental observations may be expressed by the following equation:

Table 26. Ratio of ferrous to ferric iron for 2 aged CW samples (Table 1) determined by UV-analysis.

Creek water pH	Fe^{3+}/Fe^{2+}
3.53	8.0
4.30	10.2

$$2FeSO_4 + 1/2O_2 + CaSO_4 + CO_2 \rightarrow Fe_2(SO_4)_3 + CaCO_3 \quad \text{(Eq. 3)}$$

Two sets of experiments were conducted to prevent membrane fouling and achieve 90% water recovery for the creek water aged for 60-70 days. The first set of experiments involved lowering the aged creek water temperature to reduce gypsum fouling which was based on a well-known property of increased gypsum solubility below 90 °C which reaches a maximum at 40 °C (Stephen and Stephen, 1963). Accordingly, we explored the impact of decreased creek water temperature in the 70 - 90 °C range on the water flux and recovery in batch MD tests using a fresh PP membrane.

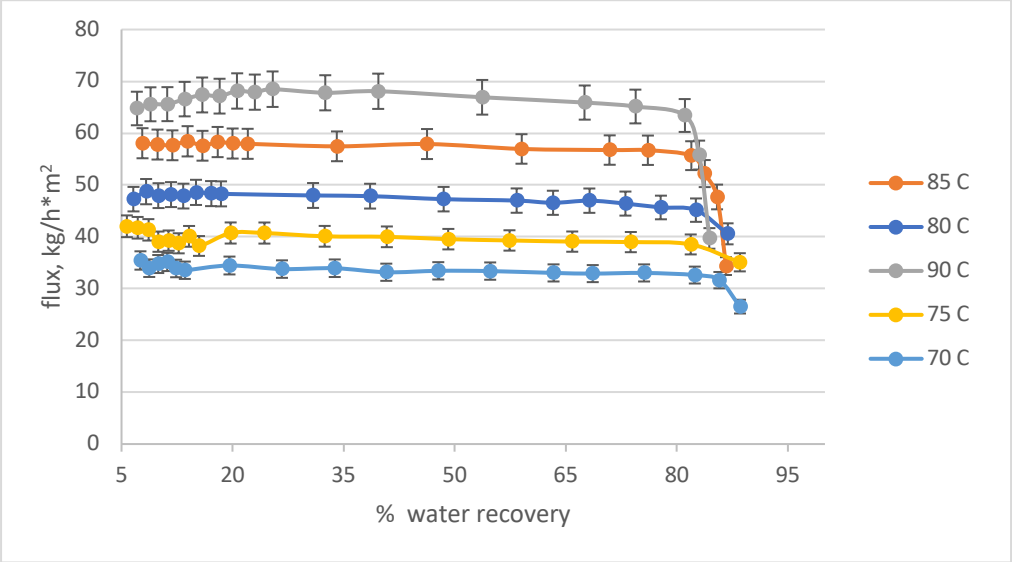

Figure 33. Water flux vs. % water recovery for aged creek water at different temperatures.

As seen in Figure 33, the MD water flux declined less significantly at greater than 60% water recovery when the aged CW temperature was below 90 °C. Although the water recovery could be increased to ~90% by lowering the CW temperature from 90 to 70 °C, there was ~48% reduction in the water flux as well as some evidence of fouling manifested in a moderate flux decline at >85% water recovery.

The second set of experiments involved chemical pretreatment of the aged creek water with highly dilute sulfuric acid to convert highly insoluble calcite into much more soluble gypsum. Moreover, according to Azimi the solubility of calcium sulfate hydrates can be also increased by the addition of sulfuric acid at elevated temperatures, which converts calcium sulfate into more soluble hydrogen sulfate, HSO_4^- (Azimi et al., 2007):

$$1^{st} \text{ dissociation: } H_2SO_4 \rightarrow HSO_4^- + H^+$$

$$2^{nd} \text{ dissociation: } HSO_4^- \rightarrow H^+ + SO_4^-$$

Moreover, at high temperatures, the second dissociation step of sulfuric acid is suppressed thereby reducing the concentration of SO_4^- ions in the solution. According to the solubility product of $CaSO_4$,

$$CaSO_4 \rightarrow Ca^{2+} + SO_4^{2-}$$

$$K_{sp\ (CaSO4)} = [Ca^{2+}]\ [SO_4^{2-}]$$

200 mg/l of Ca in the creek water will associate with 483 mg/l of sulfate to form ~0.684 g /l of $CaSO_4$ (on anhydrous basis). The addition of sulfuric acid to the aged CW will result in the association of Ca^{2+} with the HSO_4^- thereby reducing the concentration of $CaSO_4$ hydrates in the water. The solubility of $CaSO_4$ now increases because Ca^{2+} must satisfy the higher solubility product of $Ca(HSO_4)_2$ (Azimi et al., 2007). Based on experimental solubility curves of $CaSO_4$ hydrates in H_2SO_4 solutions at 95 °C reported by Azimi et al. (2007), 0.02 M of sulfuric acid was used to enhance Ca sulfate solubility in the aged creek water.

Figure 34 compares the water flux for the creek water without sulfuric acid and the creek water containing 0.02 M sulfuric acid. The increase in the TDS of the aged creek water from 900 mg/l to 10,500 mg/l is due to the addition of sulfuric acid. It is evident from Figure 34 that the addition of sulfuric acid indeed prevented fouling and rapid flux decline by converting calcite to

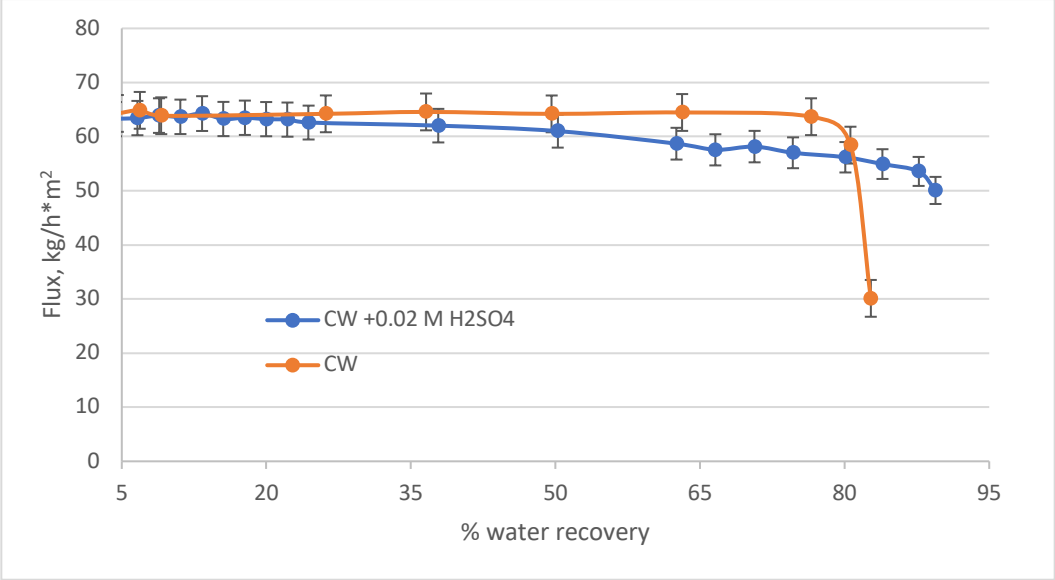

Figure 34. Water flux vs. water recovery for aged creek water (pH = 1.93 and TDS = 10,500 mg/l).

gypsum and increasing the solubility of gypsum, allowing to reach 90% water recovery for fully aged CW used as MD feed. Considering the economic costs of sulfuric acid addition, we further explored if a lower concentration of sulfuric acid (0.01 M) would be effective.

It can be seen from Figure 35 that this lower concentration of sulfuric acid is equally effective at maintaining the high water flux and achieving 90% water recovery. The change in the TDS of the creek water from 900 mg/l to 4,600 mg/l is due to the addition of sulfuric acid. The real creek water experiences rapid changes in its chemistry when stored in liquid state in air over precipitated gypsum, which has adverse impacts on the water flux due to membrane fouling. These changes are believed to be triggered by Fe^{2+} oxidation in air that eventually converts some precipitated gypsum into highly insoluble calcite that is likely to be the primary source of membrane fouling during MD. Therefore, real creek water may not be used in longer-term continuous open-loop MD tests in a lab environment without pretreatment to prevent fouling. To stabilize real creek water in our lab against adverse effects of ageing on membrane fouling, we

propose to melt, filter and pH-adjust fresh creek water with dilute H_2SO_4 to 0.01M or lower concentration prior to longer-term continuous open-loop MD tests.

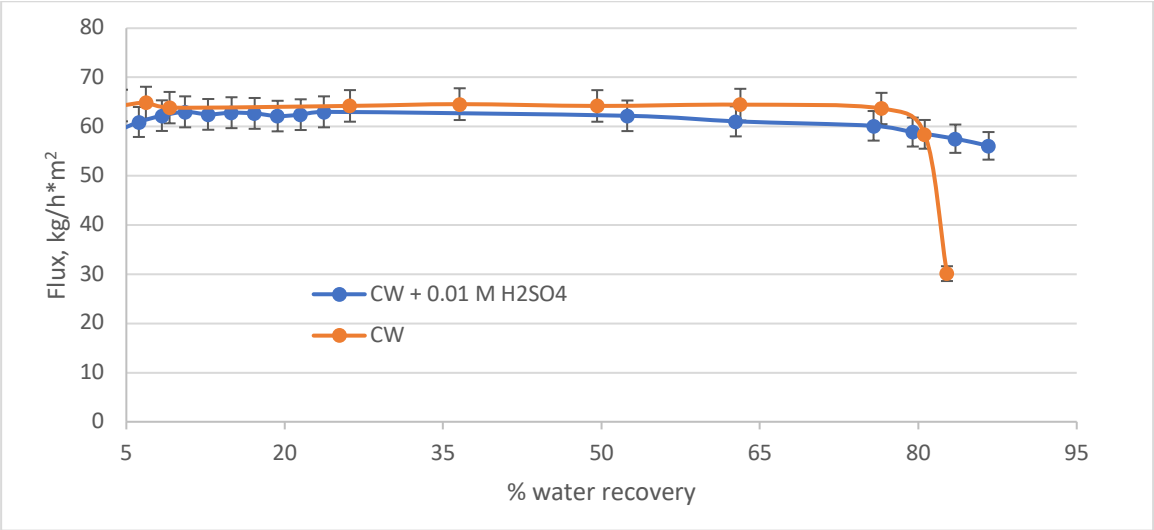

Figure 35. Water flux vs. % water recovery for aged creek water (pH = 2.20 and TDS = 4,600 mg/l).

Significant Events

1. The chemical composition of the creek water (CW) was determined by the EDS analysis of the solid obtained by CW evaporation to dryness.
2. 90% water recovery was achieved for fresh CW without a decline in water flux for the best membrane identified previously, i.e., 0.45-micron polypropylene (PP) from 3M/Cuno Company, in the batch mode under the best operating conditions.
3. CW was observed to age rapidly under ambient conditions.
4. The effect of CW ageing on the water flux in the batch MD mode was investigated.
5. CW ageing resulted in fouling and scaling of PP membrane, which was characterized by SEM and EDS.
6. Proposed fouling and scaling of the PP membrane by gypsum and calcite during MD of aged CW can be prevented by adding 0.01 M sulfuric acid, which enables reaching 90% water recovery without water flux decline.

Accomplishments

1. 90% water recovery was achieved for fresh CW without a decline in water flux using the PP membrane in the batch mode under the best operating conditions [100% accomplished].
2. Fouling and scaling associated with CW ageing was prevented by adding 0.01 M H_2SO_4, which enabled achieving 90% water recovery without flux decline [100% accomplished].

B3. Test best 0.45 μm PP membrane (3M/Cuno Co.) for up to 90 days using real Raccoon Creek AMD; Prepare detailed MD process diagrams and conduct economic analysis

The continuous open-loop MD tests were performed using the 0.45-micron pore polypropylene membrane (PP) to establish whether membrane fouling induced by the aged Raccoon Creek water could be prevented by adding diluted sulfuric acid or nitric acid. It was expected that highly insoluble calcite present in aged creek water during MD tests would be converted to relatively soluble gypsum by adding these acids.

Although the addition of sulfuric acid prevented membrane fouling during batch MD tests, it remained to be established if a similar beneficial effect of acid addition can be achieved under continuous open-loop MD conditions corresponding to highly concentrated aged creek water corresponding to 90% water recovery. Long-term continuous open-loop MD tests were performed by first conducting a batch MD test to achieve 90% water recovery. Then, deionized water was added to the concentrated feed at the same rate as it was removed from the feed during MD to the distillate stream in order to maintain the feed solute concentrations corresponding to 90% water recovery. Figure 36 shows the water flux vs. the time on stream for an open-loop continuous MD test using the creek water with 0.02 M sulfuric acid added as a feed. As Figure 36 demonstrates, the water flux gradually decreased during 300 min by ca. 20 %. The used PP membrane was characterized after MD test by Scanning Electron Microscope (SEM) and Energy Dispersive Spectroscopy (EDS) for the presence of scaling and fouling. Figure 37 shows the SEM image of feed surface of the used PP membrane after the continuous open-loop MD test using aged creek water with 0.02 M sulfuric acid added to it. The presence of extensive surface fouling is visible so that the original pore structure of a fresh PP membrane cannot be observed (Figure 37 inset). The EDS spot analysis was also performed on the feed surface revealing the presence of mostly calcium and sulfur

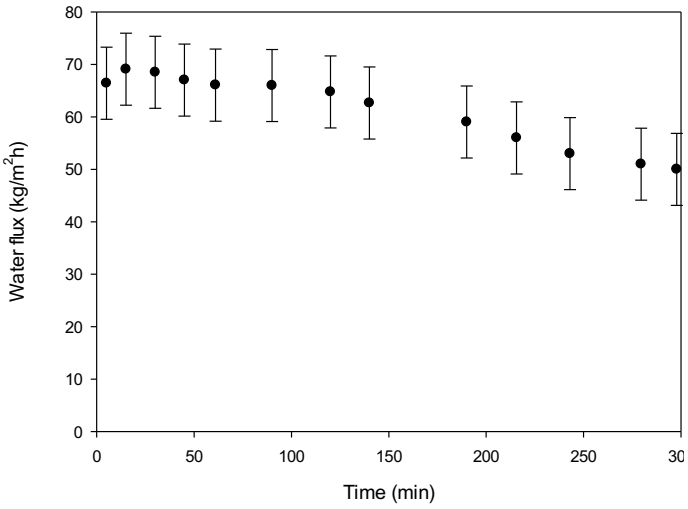

Figure 36. Water flux under continuous open-loop MD conditions as a function of time on stream using aged Raccoon Creek water containing 0.02 M sulfuric acid and TDS = 900 mg/l (prior to H_2SO_4 addition). Conditions: 0.45 micron PP membrane, 23 l/h feed and distillate flow rates, feed heater set at 90 °C, and distillate chiller at 10 °C.

corresponding to the atomic Ca/S ratio ~ 2.54, while only carbon was detected on the distillate surface.

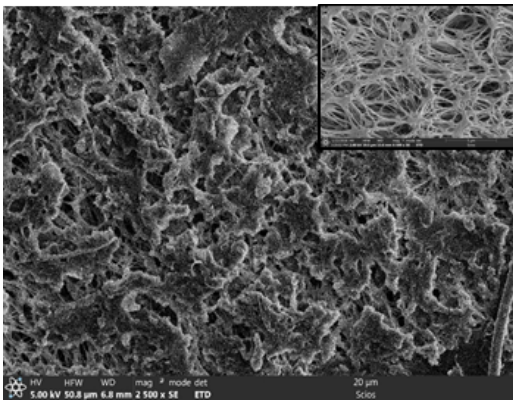

Figure 37. SEM image of a feed surface of used PP membrane after continuous open-loop MD test using aged creek water with 0.02 M sulfuric acid added. (Inset: original PP membrane) Conditions: 0.45 micron PP membrane, 23 l/h feed and distillate flow rates, feed heater set at 90 °C, and distillate chiller at 10 °C.

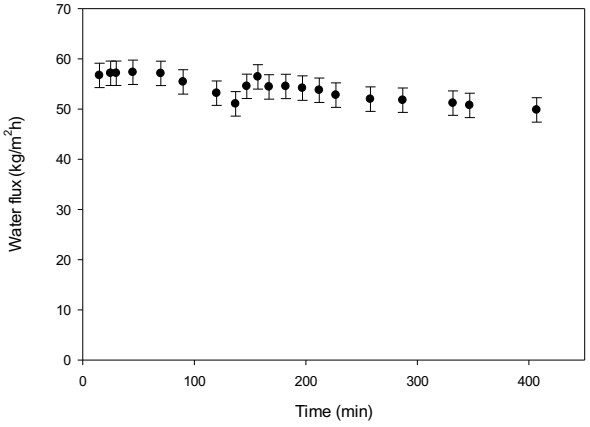

Figure 38. Water flux under continuous open-loop MD using aged Raccoon Creek water containing 0.02 M nitric acid and TDS = 900 mg/l (prior to HNO_3 addition). Conditions: 0.45 micron PP membrane, 23 l/h feed and distillate flow rates, feed heater set at 90 °C, and distillate chiller at 10 °C.

Also, the effect of 0.02 M nitric acid addition to the aged creek water on membrane fouling during continuous open-loop MD process was studied under the same MD conditions described in Figure 36. The results of this test are shown in Figure 38 that displays a similar trend to that for sulfuric acid addition and a ~ 10% reduction of water flux after 6h (~ 400 minutes) of MD testing. The used PP membrane after this MD test was investigated by SEM and EDS. Figure 39 shows the SEM image of the feed surface of used PP membrane after continuous open-loop MD test using aged creek water with 0.02 M nitric acid added to it. Similar to that for sulfuric acid addition, some surface fouling is also observed, but the open pore surface of the original membrane was still visible. The inset image shows the distillate surface of the used PP membrane showing no fouling.

However, unlike that for sulfuric acid addition, the EDS analysis indicated the presence of only carbon on both surfaces suggesting that the content of inorganic foulants was low.

Therefore, the addition of diluted acids was ineffective in maintaining high water flux during continuous open-loop MD tests because the real creek water underwent ageing that could not be prevented during its storage in the lab. In order to avoid complications from such artificial creek ageing that would not be encountered in the field, it was decided to utilize simulated Raccoon Creek water that could be made fresh as needed. Accordingly, we reviewed the historical composition data for Raccoon Creek water provided by OSMRE and found that the historical concentrations of Ca^{2+}, SO_4^{2-}, and other major ions measured at multiple locations were significantly different from those in the sample we collected in January, 2018 at Carbondale doser (FR0126 site). More specifically, the Carbondale doser sample collected in January contained untypically high Ca and sulfate concentrations as compared to the historical data for all sites, including the FR0126 site.

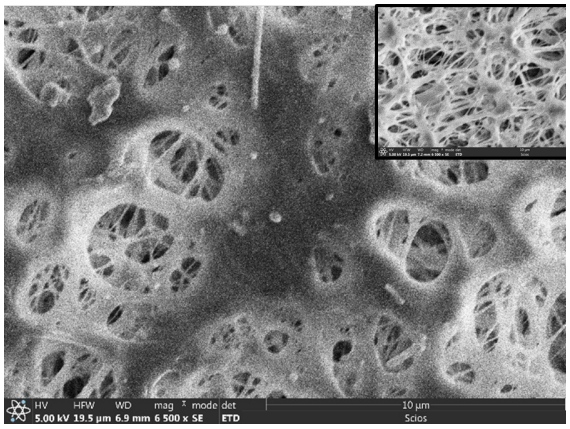

Figure 39. SEM image of a feed surface of used PP membrane after continuous open-loop MD test using aged creek water with 0.02 M nitric acid added. (Inset: distillate surface of PP membrane) Conditions: 0.45 micron PP membrane, 23 l/h feed and distillate flow rates, feed heater set at 90 ℃, and distillate chiller at 10 ℃.

Upon reviewing the historical data for Raccoon Creek, we proposed a new, representative simulated AMD composition for long-term MD tests (Table 27). The TDS content of 900 mg/l is maintained in this simulated AMD, and HCl is used to adjust its pH to pH = 2.4 and Cl^- concentration to 50.3 mg/l. In our initial continuous open-loop MD tests this simulated creek water was maintained in a 10-fold concentrated state as compared to the species concentrations shown in Table 27, which corresponded to 90% water recovery. A stable water flux of ca. 48 kg/h*m^2 was observed under these conditions (Figure 40), which is highly promising.

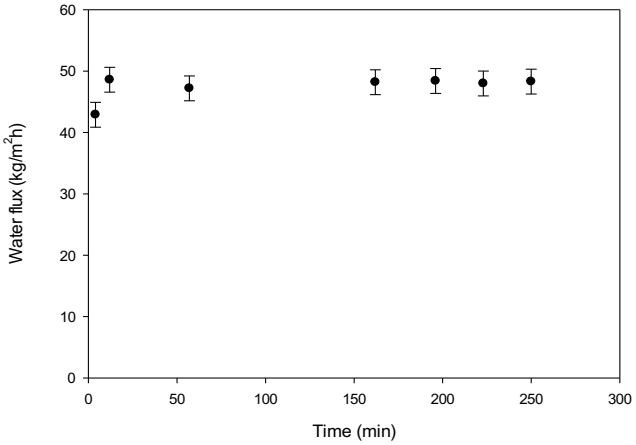

Figure 40. Water flux vs. time on stream for newly simulated Raccoon Creek water in continuous open-loop MD test. Conditions: 0.45 micron PP membrane, 23 l/h feed and distillate flow rates, feed heater set at 80 ℃, and distillate chiller at 10 ℃.

Process Economics:

The economic analysis was conducted by carrying out the steady-state mass and energy balances using PROII simulation software was updated by calculating fixed capital cost by MD performance (water flux) based on reference papers. (Khayet et. al., 2011, Tavakkoli et. al., 2017) The capital cost was calculated based on the data previously submitted. The process flow diagram (PFD) of the open-loop continuous MD process

consists of fresh AMD at 15 ℃ that is continuously fed to the feed tank, heated to 85 ℃, and pumped to the membrane housing (feed side). After passing through the membrane module the concentrated feed is fed back to the feed tank. At the same time, the pure water recovered from the feed is pumped into the distillate tank and chilled to 20 ℃. The total flow rate of AMD treated by the membrane module is 1 MGPD (million gallons per day) with 90% recovered in distillate by the MD process as pure water.

Table 27. Simulated creek water used in long-term MD studies.

Species	Concentration (mg/l)
Mg	31.0
K	4.0
Cl	50.3
Ca	50.0
Mn	14.0
Al	20.0
Fe(III)	150.0
Na	21.0
SO_4	212.5

Assumptions used in energy consumption

Heating: assumes that fresh AMD feed supplied at 1 MGPD is heated to 85 ℃; 1.024 MW

Cooling: assumes that the heat is recovered from the distillate stream (90% of the total flow rate) which is cooled from 90 to 20 ℃ by contacting it with fresh AMD at 15 ℃, while the temperature of the fresh AMD is increased to 85 ℃; 11.968 MW

Pumping**:** Two pumps (82% efficiency) pump the AMD feed and the distillate (pure water); 0.030 MW

Based on the assumptions above, the daily electricity cost for MD operating are ca. $1,745 when the industrial electricity price of $0.069/kWh was applied which was reported for Ohio in November 2017 by the US Energy Information Administration (USEIA 2017). As seen in Table 28, the capital costs decrease with increasing water flux, while the main cost factor is the membrane cost. The capital costs decrease by ca. 4% for every 10 kg/h*m^2 increase in the water flux. However, there are several scenarios that are expected to impact energy consumption in MD, which is directly related to operating costs, such as heating, cooling and electricity sources. By choosing a proper, relevant scenario, the total cost of MD process could be further optimized by balancing the capital and operating costs.

Table 28. Summary of data and assumptions used in the capital cost calculation.

	Average flux (kg/h*m^2)		
	40	**50**	**60**
Membrane needed (m^2)	4,337	3,470	2,892
Replacement per year (m^2)	867	694	578
Membrane cost	$260,247	$208,198	$173,498
Feed tank (gallons) (3 h capacity of daily flow rate)	62,500	62,500	62,500
Feed tank cost	$749,994	$749,994	$749,994
Heat exchanger cost	$230,969	$230,969	$230,969
Pump cost	$73,050	$73,050	$73,050
Total capital cost	$1,314,260	$1,262,211	$1,227,511
Yearly membrane replacement cost	$52,049	$41,640	$34,700
Yearly electricity cost	$628,200	$628,200	$628,200

Assumptions used in energy consumption:

Plant availability 90%, Electricity cost $0.069/kWh, Membrane cost $60/m^2, Membrane replacement 20%/year

Feed water storage tank 0.5 $/gal, Required heat exchanger area = Q_{hx}(kW)/U*T_{avg}, U : global heat transfer coefficient

Heat exchanger cost; $2,000/m^2

Significant Events

1) Raccoon Creek water aged rapidly which had a detrimental impact on the water flux due to membrane fouling and scaling in the batch MD mode run from 0 to 90% water recovery.
2) Membrane fouling and scaling observed during MD of the aged creek water was prevented in a batch MD mode by adding diluted sulfuric or nitric acid, which enabled reaching 90% water recovery without encountering a water flux decline.
3) Membrane fouling and rapid flux decline were observed under open-loop continuous MD conditions at 90% water recovery even after adding diluted acids to aged creek water.
4) It was decided to use a simulated composition based on the historical 2010-2016 data for Raccoon Creek recommended by Office of Surface Mining Reclamation and Enforcement (OSMRE).
5) Long-term open-loop continuous MD tests are currently being conducted employing the simulated AMD, which show a stable flux at 90% water recovery.

Accomplishments

1) Investigated membrane fouling behavior during MD of aged creek water in open-loop continuous mode. [100 % accomplished].
2) Prevented fouling and scaling in batch MD associated with ageing of the creek water by adding 0.02 M H_2SO_4 and 0.02 M HNO_3, which demonstrated the attainment of 90% water recovery without a significant flux decline. [100 % accomplished].
3) Membrane fouling and flux decline were still observed under open-loop continuous MD conditions. [100% accomplished].
4) Performed MD tests of simulated (pH adjusted) creek water in open-loop continuous MD as a function of time on stream (up to 90 days). [100 % accomplished].
5) Updated economic analysis based on energy requirements of treating 1 million gallons per day of Raccoon Creek water which were estimated by process simulations using PRO/II software. [100 % accomplished].

B4. Conduct long-term MD testing of the best 0.45 μm PP membrane (3M/Cuno Company) using simulated creek water; Conduct economic analysis of the MD process

The long-term continuous open-loop MD tests were performed daily (averaging 6 h/day) using the 0.45-micron pore polypropylene membrane (PP, 3M/Cuno Corp.) and the same simulated creek water as used previously with initial solute concentrations shown in Table 27. However, the concentrations of these solutes were 10 times higher under steady-state MD conditions corresponding to 90% water recovery. Deionized water was added to the concentrated feed using mini-peristaltic pump (Cole-Parmer) at the same rate as it was removed from the feed to the distillate by the MD membrane in order to maintain the feed solute concentrations at levels corresponding to 90% water recovery.

Figure 41 shows a daily average water flux and total dissolved solids (TDS) as a function of time on stream for an open-loop continuous MD test described above. As Figure 41 demonstrates, the water flux decreased during the first few days and then stabilized showing the average water flux of 45 kg/h*m^2. The membrane was treated periodically with 0.1 M nitric acid as indicated by arrows in Figure 41 to remove the foulants and regenerate the membrane. The acid wash was performed only on the feed side of the membrane at 10 l/h and room temperature and lasted for one hour. After the acid wash the membrane was washed with deionized water prior to the next run using a fresh batch of simulated wastewater. During the first 15 days of operation, the water flux of 45 kg/h*m^2 was recovered after every nitric acid wash. However, after that time on stream the water flux declined more significantly and could no longer be recovered by nitric acid washes, while the TDS levels increased in the distillate indicating that the feed solution penetrated from the feed to distillate side. Therefore, at that point it was decided to stop these longer-term tests, remove the PP membrane from the permeation cell, and characterize it by SEM and EDS for the presence of scaling and fouling on the membrane surface.

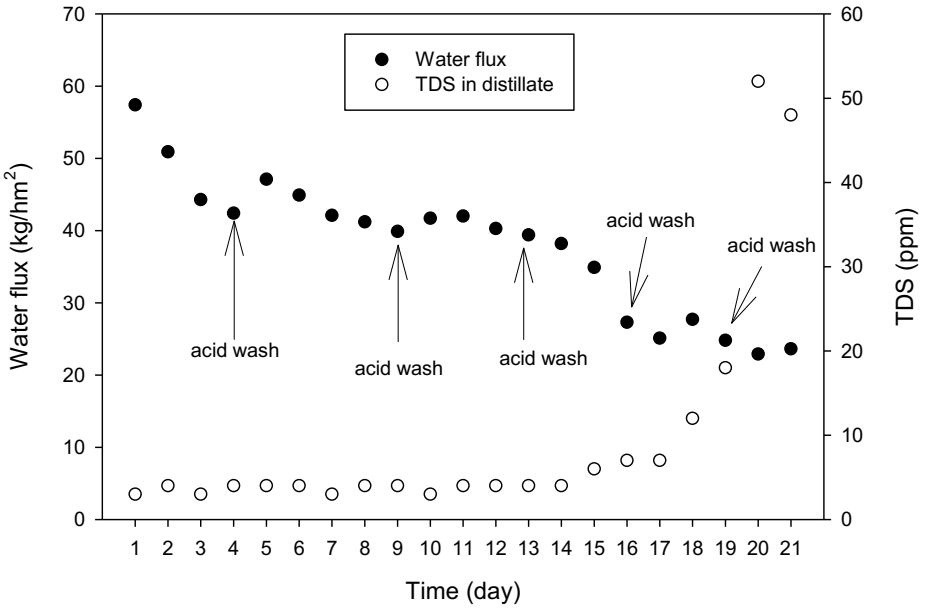

Figure 41. The daily average water flux and TDS levels in the distillate as a function of time on stream under open-loop MD conditions using simulated Raccoon Creek water (Table 27). Conditions: 0.45 micron PP

It should be noted that MD membranes cannot be removed from the permeation cell without damage. Therefore, once a membrane is removed from the permeation cell, it can no longer be used in permeation tests. Moreover, it is not possible to characterize the membrane fouling during longer-term permeation tests shown in Figure 41. Instead, we conducted a short-term (3 days) open-loop MD permeation and fouling test using a fresh PP membrane under the same process conditions as those reported in Figure 41. The used membrane after this short-term test was washed with *deionized water (DI)* and characterized by SEM and EDS (Figure 42). Two different types of deposits were observed by SEM: (1) a small number of large particles located on the membrane surface (Figure 42 (a)), and (2) many small particles covering the entire membrane surface on the feed side (Figure 42 (b)). The EDS analysis of several fouled areas of the membrane surface indicated that the large particles contained mostly iron oxide with a small amount of sulfur corresponding to the atomic Fe/S ratio 6-10. The iron oxide (FeO_x) particles were also observed to form on internal surfaces of plastic tubing used in the MD setup as well as to be deposited on the membrane surface during the short-term MD test. Although these iron oxide particles could not be removed by washing with DI water, the formation of these particles was too limited to be responsible for the flux decline during longer-term MD tests. The second type of deposits were observed as a dense layer of small iron-containing particles characterized by a higher sulfur content (the atomic Fe/S ratio of 0.8-2.7) apparently corresponding to iron (oxy) sulfate that dissolved in dilute nitric acid. It should be noted that Liu et al. (2006) successfully used dilute nitric acid in a chemical treatment procedure for PP membranes.

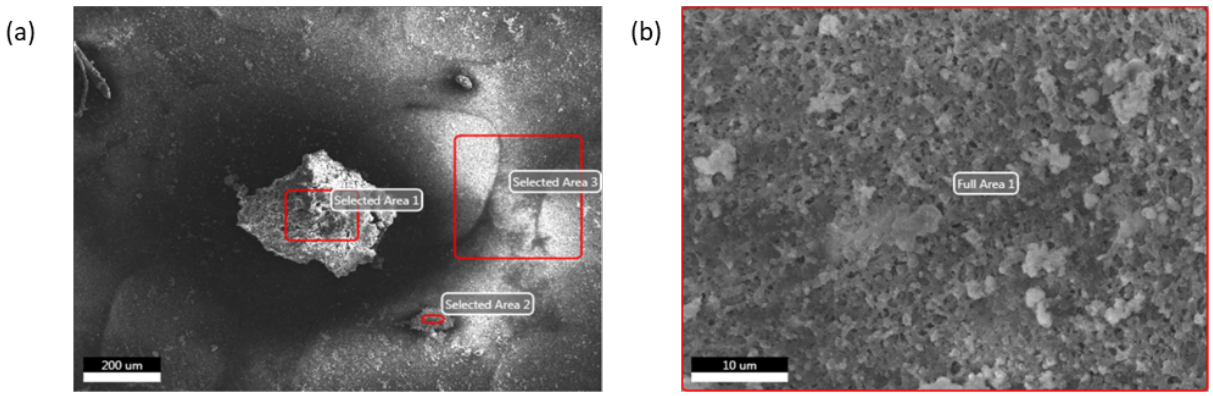

Figure 42. SEM image of the foulant particles deposited on a feed surface of used PP membrane after 3 days of open-loop MD testing using simulated Raccoon Creek water (Table 27). Conditions: 0.45 micron PP membrane (3M/Cuno); 23 l/h feed and distillate flow rates; feed heater set at 90℃, and distillate chiller at 10℃.

The deposited foulant particles were successfully removed by *acid wash* as shown in Figure 43. Figure 43 shows the SEM image of the feed surface of the used PP membrane after 21 days of open-loop MD testing (Figure 41) that employed simulated creek water (Table 27) concentrated 10-fold. This used membrane was washed by 0.1 M nitric acid before it was removed from the housing which was apparently effective at removing extensive surface fouling previously observed (Figure 42 b) as the open pore structure was clearly visible (Figure 43). This confirmed that the chemical treatment with 0.1 M nitric acid flowing at 10 l/h for 1 h at room temperature is highly effective at removing the foulants from the PP membrane surface.

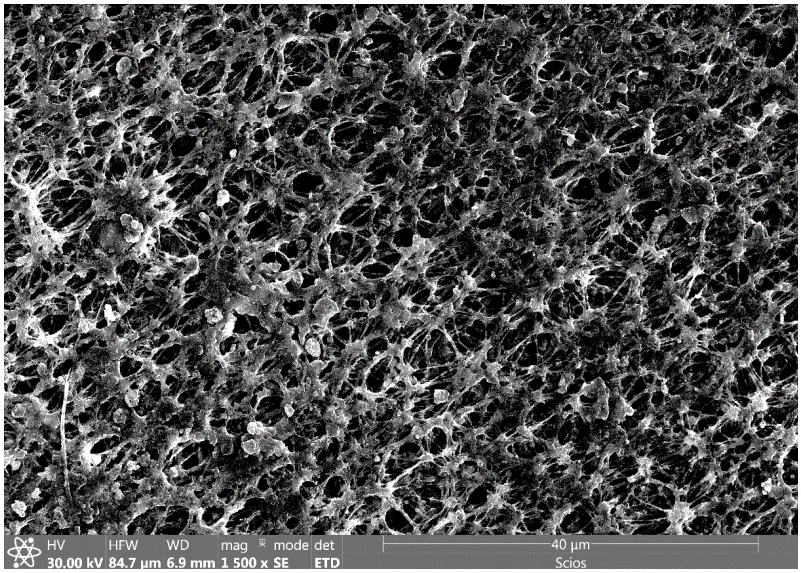

Figure 43. SEM image of the feed surface of used PP membrane regenerated by 0.1M nitric acid wash. This membrane underwent 21 days of open-loop continuous MD testing (Figure 41) using simulated creek water (Table 27) concentrated 10-fold. Conditions: 0.45 micron PP membrane; 23 l/h feed and distillate flow rates; feed heater set at 90°C, and distillate chiller at 10°C.

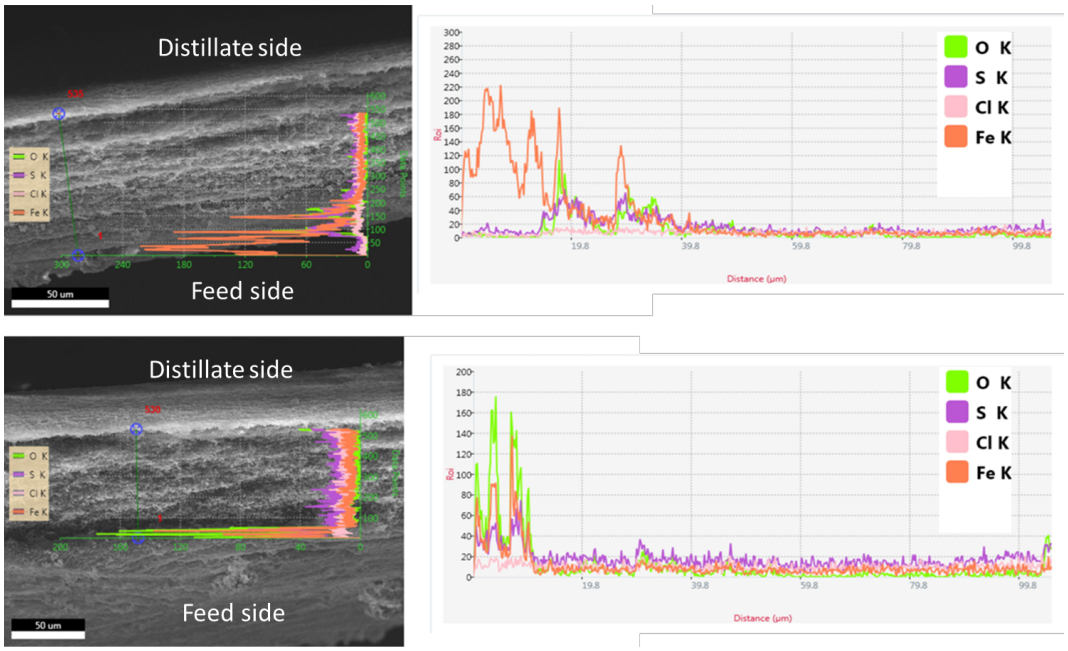

Figure 44. SEM image and cross-sectional elemental analysis of used PP membrane regenerated by 0.1M nitric acid wash after 21 day open-loop MD test using simulated Raccoon Creek water (Table 27) concentrated 10-fold. Conditions: 0.45 micron PP membrane; 23 l/h feed and distillate flow rates; feed heater set at 90 °C; and distillate chiller at 10 °C.

However, the water flux data shown in Figure 41 indicated that after 18 days of longer-term MD testing the average water flux of 45 kg/h*m^2 could no longer be recovered after the acid

wash despite the feed surface being visibly free from the foulant particles (Figure 43). To elucidate the cause of these irreversible flux changes, we performed a cross-sectional SEM and EDS analysis of this acid-washed PP membrane after 21 days on-stream. Figure 44 shows the cross-sectional EDS elemental analysis of this used PP membrane for two different spots, which indicated the presence of iron, together with sulfur and oxygen, and suggested iron penetration from the feed to distillate side. The penetration depth varied from 10 to 25 μm which is approximately one third of the membrane thickness. These results suggested that the PP membrane surface probably lost its hydrophobic character due to fouling and/or nitric acid wash which led to surface wetting and feed percolation and lowered the water flux and transported solutes from the feed to the distillate side. As shown in Figure 41, TDS content progressively increased in the distillate after 15 days of MD operation, which supports this conclusion. According to Guillen-Burrieza et. al. (2014), organic acids, such as oxalic and citric acids and their mixtures are better at membrane cleaning than strong mineral acids, and are more benign. However, to prevent detrimental wetting of the membrane surface, acid wash combined with a membrane drying step would be essential for a complete membrane regeneration.

Process Economics:

The process flow diagram (PFD) shown in Figure 45 was developed based on the MD data obtained in this project in order to determine the energy requirements for the MD process to treat AMD.

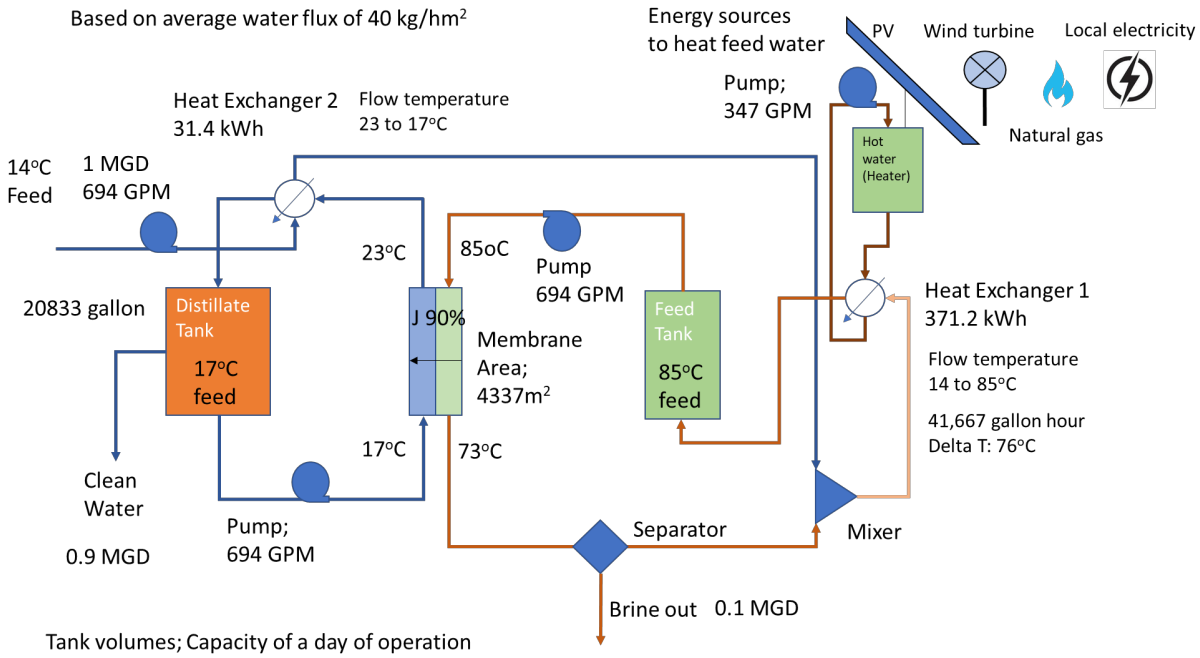

Figure 45. PFD of proposed open-loop continuous MD system to recover clean water from AMD.

The proposed process is designed to treat 1 million gallons of AMD per day supplied at 14 °C, heated to 85 °C using 4 different energy sources, and transferred to the hot feed tank. 0.9 million gallons per day of pure water at 17 °C from the MD process will be discharged while collecting 0.1 million gallon per day of brine for disposal. The MD feed and distillate streams will be maintained at 85-73 °C and 23-17 °C, respectively. Pure water generated by the MD process can be used as irrigation water. However, in this study we assumed that pure water will be discharged into a nearby body of water, while the brine disposal will be location-dependent. PRO/II simulation software (Schneider Electric) was used to calculate the energy demand of the MD process and evaluate process economics.

The cost analysis of the MD plant was performed for two major components of capital cost and annual operating cost. The capital cost was defined as the cost associated with plant

Table 29. Summary of parameters used in the fixed capital cost calculation.

Plant life time	20 years
Plant capacity	1,000,000 gal/day
Plant availability	90%
Site development	$\$26.42/m^3/day$
Interest rate	5%
Amortization factor	0.08
Electricity cost	\$0.069
MD PP membrane cost	$\$53.80/m^2$
Membrane replacement	20 ~ 1,200 %/year
Membrane module	$\$360/m^2$
Feed and Permeate storage tank	\$0.45/gal
Heat exchanger cost	a. Heat exchanger 72 m^2; \$15,487 b. Heat exchanger 157.7 m^2; \$15,487
Pump cost	a. High speed (157.7 m^3/h); \$15,487 b. Low speed (78.9 m^3/h); \$10,804
Installation, **Instrumentation and control cost**	25% of the purchased equipment cost (Banat and Jwaied, 2008; Peter et al. 2003)

construction, process equipment purchases, and installation charges. Land cost was assumed to be zero due to US federal government ownership of the AMD treatment site. The operating costs included amortization, fixed charges, operating and maintenance (O&M) costs, and membrane replacement costs. Separate cost analysis was conducted for 4 different heating sources and included in annual operating costs. Various parameters used in the fixed capital cost calculation that depended on the process capacity and design features are summarized in Table 29 and discussed below:

- *Site development*

  A one-time site development cost incorporated costs associated with buildings, roads, fences, and other modifications required for installation (Sirkar and Song, 2009). The site development cost for this hybrid process was assumed to be \$26.42/m^3/day (Tavvakoli et al. 2017).

- *Pumps and heat exchangers*

  The essential information regarding the energy and material balances to calculate capital and operational costs were derived from PRO/II simulations. The unit prices for pumps and other equipment were calculated based on cost curves published by National Energy Technology Laboratory (NETL) dating back to the base year of 1998 (Loh, 2002) and adjusted for inflation to 2018 prices using the US inflation calculator (Coinnews Media Group 2018).

- *Membrane-associated costs*

$$membrane\ area\ required\ (m^2) = \frac{permeate\ mass\ flow\ rate\ \left(\frac{kg}{hr}\right)}{flux\ \left(\frac{kg}{m^2 hr}\right)} \quad (1)$$

  The membrane area was calculated using Equation (1). The required membrane area was approximately 4,337 m^2 based on the average MD water flux of 40 kg/h*m^2. The MD membrane module cost was also considered based on a literature value for plate-and-frame Direct Contact MD (DCMD) systems (Sirkar and Song, 2009; Tavvakoli et al. 2017).

- *Storage tanks*

  Storage tanks were priced based on plant capacity and the recovery factor assuming that feed water and purified water can be retained for one day of operation. Storage tank prices were obtained and considered based on literature value for the desalination process to treat high-salinity shale-gas produced water (Saffarini et al., 2012).

- *Operating and maintenance (O&M) costs*

  O&M costs included plant commissioning and operation costs, i.e., for energy (thermal and electricity), spares, labor, pretreatment, filtration, and membrane replacement. The O&M costs were estimated as 20% of plant annual payment (Sirkar and Song, 2009; Tavvakoli et al. 2017), while no pretreatment and filtration of feed was considered for this MD process. Also, interest charges on project fund loans were added to operating costs as a fixed cost calculated by

multiplying the capital cost by an amortization factor *a*, which is given by eq. (2) where *r* and *n* are defined as the discount rate and number of future payments over a defined period of time, respectively:

$$a = \left(\frac{r(1+r)^n}{(1+r)^n - 1} \right) \qquad (2)$$

It should be noted that the membrane replacement rate depends on the feed water quality. A literature review has shown the annual membrane replacement to be approximately 20% for high salinity wastewater, such as AMD (Sirkar and Song, 2009; Tavvakoli et al. 2017). The total annual cost was obtained by adding annual fixed, O&M and membrane replacement costs.

- *Sensitivity studies*

The cost sensitivity studies were performed by considering different energy sources to heat the AMD feed. Two different scenarios were considered based on site location. The first scenario assumed a remote location without an access to electric utility. In this case photovoltaic (PV), solar thermal, wind turbine and standalone natural gas tank heater were considered. If the site is on infrastructure-accessible location, then a local electric utility or natural gas line would be significant energy sources, either alone or in combination with (renewable) energy sources mentioned above. The cost analysis for these different energy sources was performed based on 2018 Annual Technology Baseline reported by National Renewable Energy Laboratory (NREL) (ATB-NREL 2018). The Levelized Energy Costs (LEC) of each energy source were recalculated for each scenario and summarized in Table 30.

Table 30. Levelized energy costs by energy source.

Case 1	MD standalone using local electricity	$0.069/kWh
Case 2	MD + Photovoltaic (PV)	$0.218/kWh
Case 3	MD + Solar Thermal	$0.167/kWh
Case 4	MD + Wind Turbine	$0.077/kWh
Case 5	MD + Steam (natural gas combustion, NG)	$0.039/kWh
Case 6	MD + PV + Wind Turbine (50%)	$0.148/kWh
Case 7	MD + steam (30%) + PV	$0.164/kWh
Case 8	MD + steam (30%) + Wind Turbine	$0.066/kWh

Based on these costs, only natural gas is a cheaper option to heat AMD feed as compared to local electric utility. However, if the MD process location is remote, a stand-alone natural gas supply is required to provide ca. 107 gallons/day of liquified natural gas. In this case, the natural

Table 31. Total process costs for MD system.

Capital and Operating and Maintenance Costs	
Site development	$100,000
Membrane	$232,030
Membrane module	$1,561,320
Heat Exchangers	$348,000
Pumps	$57,265
Tanks	$1,349,978
Indirect cost	$729,719
Installment cost	$1,094,578
Instrument and control cost	$1,094,578
Membrane replacement	$46,406
Annual fixed charges	$351,327
Operating and maintenance	$70,265
Fixed process cost per volume of treated AMD water	$0.393/$m^3$

gas cost included monthly trucking costs of ca. 3,499 gallons/tanker truck. In terms of natural gas consumption and its expected future price increases, natural gas consumption was set for a maximum of 30% of total energy required, while the rest of this energy was assumed to be provided by solar and wind. Also, natural gas LEC is expected to increase annually and almost doubled by 2040 (Electricity Generation Baseline Report, EGBR, 2017).

The itemized fixed process costs are summarized in Table 31. The membrane module and storage tanks are the two major items with the greatest impact on capital costs, while additional operating energy costs for each case are listed in Table 30. The membrane replacement is another major contributor to maintenance costs that depend on the replacement frequency.

The total fixed process cost per treated AMD volume is ca. $0.393/$m^3$ as shown in Table 31. We conducted a sensitivity study (Table 30, Cases 1-8) for different energy sources to better understand their impacts on the total MD process cost. The total process costs per volume of treated AMD for each case are shown in Figure 46.

According to Figure 46, the most expensive energy to drive the MD system is solar thermal energy, while PV is the second most expensive. The AMD water treatment cost per unit volume is ca. 2.8 times higher for case 2, the solar thermal energy, as compared to case 5, pipelined natural

gas, while case 3, the PV energy, is ca. 2.3 times more expensive than pipelined natural gas. However, as shown in Figure 47 (ATB-NREL, 2018; EGBR, 2017), the renewable energy costs, especially those for PV, are projected to decrease appreciably over the next 10 years. The LEC of PV, wind turbine and natural gas energy are expected to be similar by 2030, because of the decreasing LEC of renewable energy and increasing LEC of natural gas.

We considered one more case, i.e., the impact of the membrane replacement frequency on the total MD process costs, because this frequency depends on the rate of irreversible membrane fouling. The membrane replacement frequency in this case was varied from 20 to 1,200%, the latter number corresponding to monthly membrane replacement. However, the membrane replacement cost had a relatively minor impact on the total process cost at up to 100% of membrane replacement (i.e., once a year), while monthly membrane replacement is expected to increase the total cost by 8.4% for case 2 (minimum) to 23.6% for case 5 (maximum). Furthermore, in 2030, when the renewable energy and natural gas price are expected to be similar, the AMD treatment cost would be \$ 0.702/m^3. This cost could be lowered further if the pure process water could be used for a practical purpose, such as irrigation water.

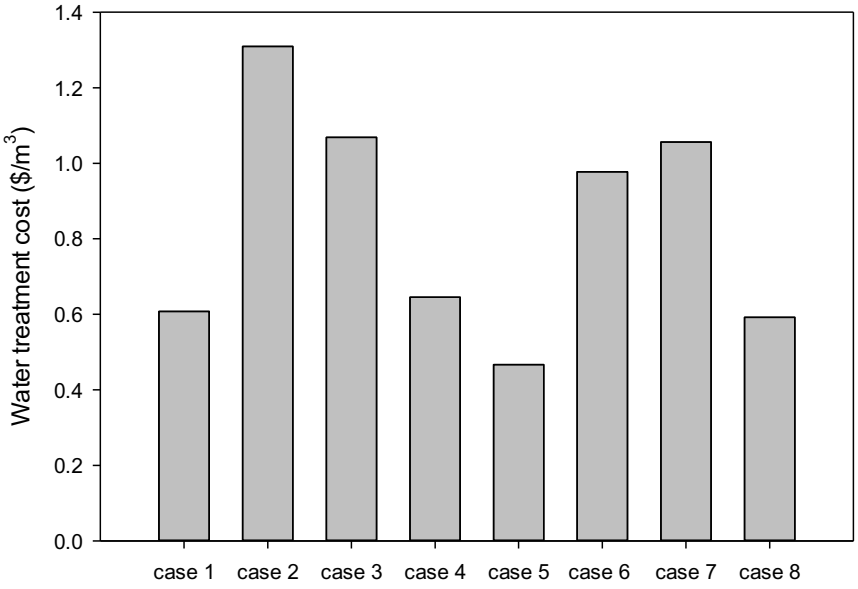

Figure 46. The cost sensitivity study for different energy sources used to drive the proposed MD process (per AMD volume treated). Case 1: local electricity; Case 2: PV; Case 3: MD Solar Thermal; Case 4: Wind Turbine; Case 5: Steam (NG): Case 6: 50% PV and 50% wind; Case 7: Steam (30%) and PV (70%) Case 7: Steam (30%) and wind (70%). For Case 5, natural gas was supplied by a pipeline, while for Cases 7 and 8, 30% steam in a hybrid system is generated by burning natural gas supplied in a standalone tank.

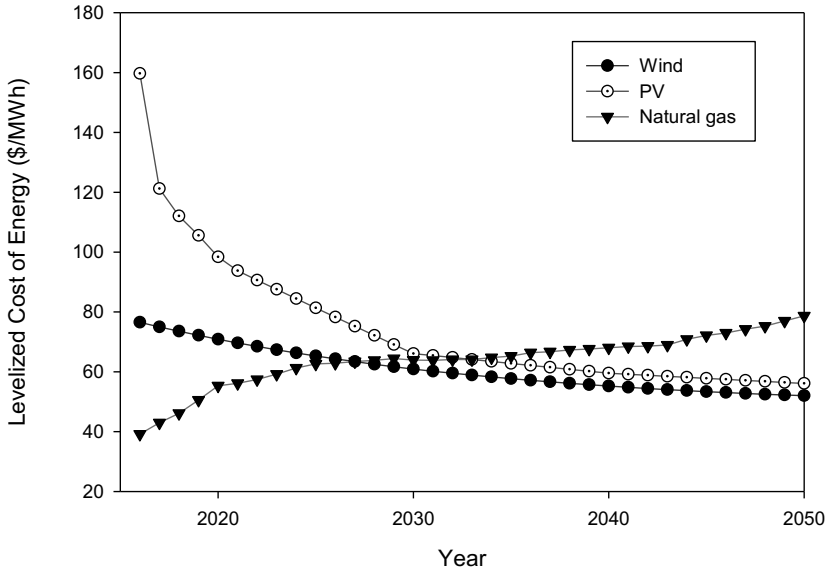

Figure 47. LEC projections for natural gas and renewable energy sources (2016 - 2050).

Lastly, we compare these costs with projected costs of chemical treatment of AMD combined with costs of floc handling and disposal (Skousen, 2014). These costs for three least expensive chemicals used in the AMD neutralization are shown in Table 32.

Table 32. Current cost estimates of chemical treatment of simulated Raccoon Creek AMD (pH 2.4).

Parameter	Limestone	Hydrated Lime	Pebble Quicklime
Conversion Factor (CF)*	1	0.74	0.56
Neutralization Efficiency (NE)	30%	90%	90%
2018 Cost, $/ton[&]	40	150-320	230-340
H_2SO_4, ton/yr	599	599	599
Chemical, ton/yr	1,996	492	373
Chemical, ton/day	5.47	1.35	1.02
Chemical (FOB), $/m^3 AMD	0.058	0.053-0.114	0.051-0.075
Chemical (FOB + US rail), $/m^3 AMD[@]	0.220	0.093-0.154	0.081-0.105
Total Cost (including floc), $/m^3 AMD[#]	0.880	0.372-0.616	0.324-0.420

* Tons of acid/yr = AMD flow (gpm) x AMD acidity (mg/l) x 0.0022

Tons of chemical/yr = Tons of acid/yr x CF / NE

AMD flow = 1,000,000 gpd = 694 gpm AMD acidity = pH 2.4 = 0.004 M H_2SO_4 = 392 mg/l

[&] quoted on Alibaba as free on board (FOB) price

[@] US rail shipping costs of $0.051/ton-mile (Austin, 2015) used to estimate costs to transport bulk chemicals from the Long Beach Terminal to Ohio (2,200 mi).

These estimates demonstrate that the total treatment costs of $0.476/m^3 of AMD by the MD technology are comparable or appreciably better than the estimates of these costs for the chemical treatment and floc disposal ($0.324-$0.880/m^3 of AMD) using relatively inexpensive neutralization chemicals, such as limestone, hydrated lime and pebble quicklime. This cost comparison further indicated that the novel open-loop continuous MD process is expected to be attractive from both the economic and environmental perspectives.

Significant Events

1) Membrane fouling by iron oxide could be removed by washing the membrane with dilute nitric acid (0.1M) for one hour at room temperature supplied at a flow rate of 10 l/h.
2) Water flux was maintained for 15 days of open-loop continuous MD operation with periodic nitric acid washing.
3) The water flux decreased by ca. 30% and could not be recovered after washing with dilute nitric acid after 15 days of operation.
4) Whereas the surface foulants were completely removed from the PP membrane by a nitric acid wash, the membrane lost its hydrophobic character resulting in feed wetting, percolation and reduced water flux.
5) The PP membrane maintained water flux for 15 days on stream. However, due to unavailability of fresh natural AMD on a daily basis in this longer-term study, a 10-fold concentrated simulated feed was used instead. The contact volume of this feed normalized to membrane area and time was 371 l/h m^2, while in a full-scale process, this parameter is expected to be ca. 10 times lower (36.4 l/h m^2). This indicated ~10 times slower membrane fouling rate and the PP membrane replacement once every 150 days under real process conditions, which is expected to result in a relatively minor increase in the overall process costs.
6) The economic analysis indicated pipelined natural gas and local electricity to be the most economical energy sources that result in total treatment costs of $ 0.476/m^3 and $0.607/m^3, respectively. The former cost is expected be ca. 7.6% higher if the PP membrane is replaced every 150 days. However, by 2030 these AMD treatment costs are expected to be comparable to the costs based on renewable energy ($ 0.702/m^3) due to increasing natural gas prices and decreasing renewable energy costs, especially for PV.
7) The MD process costs are expected to be comparable or lower than the combined costs of chemical treatment and floc disposal methods ($0.324-$0.880/m^3 of AMD).

Accomplishments

1) Performed tests of pure water recovery from simulated creek water in open-loop continuous MD as a function of time on stream (20 days). [100 % accomplished].
2) Investigated membrane fouling behavior during MD of simulated creek water in open-loop continuous mode. [100 % accomplished].
3) Conducted detailed economic analysis of proposed MD process to treat AMD based on energy requirements of treating 1 million gallons per day of creek water which were estimated by process simulations using PRO/II software. [100 % accomplished].

CONCLUSION

This applied science project explored the techno-economic feasibility of a new MD process to selectively remove >90% of water from AMD and concentrate TDS employing five promising commercial membranes (two PP, two PTFE and one PVDF). Among all commercial membranes tested, 0.45 μm pore PP membrane exhibited the highest water flux (ca. 62 kg/h*m^2) and achieved 90% water recovery under optimal open-loop continuous MD conditions employing a realistic simulated AMD feed (TDS = 900 mg/l, pH = 2.4). According to these tests, the PP membrane would need to be replaced once every 150 days under real process conditions.

Our economic study of a scaled up open-loop continuous MD process to treat 1 million gallons of AMD per day indicated that such frequency of membrane replacement is expected to have a minor impact on the overall process economics. The cost analysis of the MD plant was performed for two major components of capital cost and annual operating cost, and for four different energy sources, including local utility, photovoltaic, solar thermal, wind, and natural gas. The economic analysis indicated pipelined natural gas and local electricity to be the most economical energy sources for heating AMD water that result in the total treatment costs of \$0.476/m^3 and \$0.607/m^3 of AMD, respectively. However, by 2030 these AMD treatment costs are expected to be comparable to the costs based on renewable energy (\$0.702/m^3) due to increasing natural gas prices and decreasing renewable energy costs, especially for PV.

Furthermore, these MD process costs are competitive with our estimates of combined costs of chemical treatment and floc handling and disposal of precipitated metal hydroxides (\$0.324-\$0.880/m^3 of AMD). Therefore, pilot-scale studies of this new promising MD technology are proposed as the next step in its development and commercialization to recover pure water and concentrate TDS in AMD.

REFERENCES

A. Alkhudhiri, N. Darwish, N. Hilal, Desalination 287 (2012) 2.

A.M. Alklaibi, N. Lior, J. Membr. Sci. 255 (2005) 239.

Annual Technology Baseline 2018 - 2018 ATB – NREL, https://atb.nrel.gov/

D. Austin, Working Paper 2015-03, Congressional Budget Office, Washington, DC, March, 2015, http://www.iemonitor.com/files/CBO%20freight%20costs.pdf

G. Azimi, V.G Papangelakis, J.E Dutrizac, Fluid Phase Equil. 260 (2007) 300.

F. Banat, N. Jwaied, Desalin. 220 (2008) 566.

S. Al-Obaidani, E. Curcio, F. Macedonio, G.D. Profio, H. Al-Hinai, E. Drioli, J. Membr. Sci. 323 (2008) 85.

COINNEWS Media Group LLC (accessed October 18, 2018), US Inflation Calculator, https://www.usinflationcalculator.com/

T.-C. Chen, C.-D. Ho, H.-M. Yeh, J. Membr. Sci. 330 (2009) 279.

A. Criscuoli, M.C. Carnevale, E. Drioli, Chem. Eng. Process. Process Intensif. 47 (2008) 1098.

H. C. Duong, A. R. Chivas, B. Nelemans, M. Duke, S. Gray, T. Y. Cath, L. D. Nghiem, Desalination 366 (2015) 121.

EGBR, J. Logan, C. Marcy, J. McCall, F. Flores-Espino, A. Bloom, J. Aabakken, W. Cole, T. Jenkin, G. Porro, and C. Liu (NETL), F. Ganda (ANL), R. Boardman (INL), T. Tarka, J. Brewer and T. Schultz (NETL), Technical Report NREL/TP-6A20-67645 January 2017.

L. Eykens, K. De Sitter, C. Dotremont, W. De Schepper, L. Pinoy and B. Van Der Bruggen, Appl. Sci. 7 (2017) 118.

A.G. Fane, R.W. Schofield, C.J.D. Fell, Desalin. 64 (1987) 231.

A.C.M. Franken, J.A.M Nolten, M.H.V. Mulder, D. Bargeman and C A. Smolders, J. Membr. Sci, 33 (1987) 315.

E. Guillen-Burrieza, A. Ruiz-Aguirre, G. Zaragoza, H.A. Arafat, J. Membr. Sci. 468 (2014) 360.

T.E. Higgins *et al.*, "Flue Gas Desulfurization Wastewater Treatment Primer", Power Magazine, March 1, 2009.

J. A. Jacobs and S. M. Testa, "*Acid Mine Drainage, Rock Drainage, and Acid Sulfate Soils: Causes, Assessment, Prediction, Prevention, and Remediation*", 1st Ed., J. A. Jacobs, J. H. Lehr, and S. M. Testa, Eds., John Wiley & Sons, Inc., 2014, Ch. 1, p. 3.

JCPDS — International Centre for Diffraction Data Sample Preparation Methods in X-Ray Powder Diffraction. Powder Diffr. 1 (1986) 51.

M. Khayet, T. Matsuura, "*Membrane Distillation: Principles and Applications"*, Elsevier, ISBN 0444531262, 2011.

M. Laqbaqbi, J. A. Sanmartino, M. Khayet, C. García-Payo, M. Chaouch, Appl. Sci. 7 (2017) 334.

C. Liu, S. Caothien, J. Hayes, T. Caothuy, T. Otoyo, T. Ogawa, "Membrane chemical cleaning: From art to science", January 2006, available online: https://www.researchgate.net/publication/242100028_Membrane_Chemical_Cleaning_From_Art_to_Science.

H.P. Loh, *Process Equipment Cost Estimation Final Report*, January 2002, DOE/NETL-2002/1169.

R. Lovett and P. Ziemkiewicz, "*Calcium peroxide for treatment of acid mine drainage*". In: Proceedings of the 2nd International Conference on the Abatement of Acidic Drainage. MEND, CANMET, Montreal, QC, Canada, 1991, pp. 35–46.

D. R. Neuman, P. J. Brown, and S. R. Jennings, "*Acid Mine Drainage, Rock Drainage, and Acid Sulfate Soils: Causes, Assessment, Prediction, Prevention, and Remediation*", 1st Ed., J. A. Jacobs, J. H. Lehr, and S. M. Testa, Eds., John Wiley & Sons, Inc., 2014, Ch. 13, p. 139.

M. S. Peters, D. K. Timmerhause, and R. E. West, Plant Design and Economics for Chemical Engineers, 5th Ed., McGraw Hill, New York, 2003.

R.B. Saffarini, E.K. Summers, H.A. Arafat, J.H. Lienhard V, Desalin. 299 (2012) 55.

S. Shirazi, C.-J. Lin, D. Chen, Desalination 250 (2010) 236.

K.K. Sirkar, L. Song, *Pilot-scale Studies for Direct Contact Membrane Distillation based Desalination Process*, US Department of the Interior, Bureau of Reclamation, 2009. https://www.usbr.gov/research/AWT/reportpdfs/report134.pdf

J. Skousen, "*Acid Mine Drainage, Rock Drainage, and Acid Sulfate Soils: Causes, Assessment, Prediction, Prevention, and Remediation*", 1st Ed., J. A. Jacobs, J. H. Lehr, and S. M. Testa, Eds., John Wiley & Sons, Inc., 2014, Ch. 29, p. 327.

S. Srisurichan, R. Jiraratananon, A.G. Fane, J. Membr. Sci. 277 (2006) 186.

H. Stephen and T. Stephen, *Solubilities of Inorganic and Organic Compounds*, Vol. 1, Macmillan, New York, 1963.

S. Tavakkoli, O. R. Lokare, R. D. Vidic, V. Khanna, Desalin. 416 (2017) 24.

USEIA (2017), US Energy Information Administration, https://www.eia.gov/ forecasts/steo/report/electricity.cfm.

USEPA (2003): http://water.epa.gov/type/watersheds/monitoring/upload/2003_03_17_monitoring_elements_elements03_14_03.pdf

USEPA method 200.8, revision 5.4, 1994

USEPA (2009), "Steam Electric Power Generating Point Source Category: Final Detailed Study Report", EPA 821-R-09-008, October, 2009.

USEPA (2011), "2011 Edition of the Drinking Water Standards and Health Advisories".

USEPA (2012a): http://water.epa.gov/drink/contaminants/index.cfm#Inorganic

USEPA (2012b): http://www.epa.gov/acidrain/effects/surface_water.html

USEPA (2017), EPA Secondary Maximum Contaminant Levels: A Strategy for Drinking Water Quality and Consumer Acceptability, https://www.epa.gov/dwstandardsregulations/secondary-drinking-water-standards-guidance-nuisance-chemicals

D. M. Warsinger, J. Swaminathana, E. Guillen-Burrieza, H. A. Arafat, J. H. Lienhard, V, Desalin. 356 (2015) 294.

World Health Organization (WHO, 2017), *Guidelines for drinking-water quality: 4th edition incorporating the first addendum*, ISBN: 978-92-4-154995-0

K. Zhao, W. Heinzl, M. Wenzel, S. Büttner, F. Bollen, G. Lange, S. Heinzl, N. Sarda, Desalin. 323 (2013) 150.